# A Novel Non-contact Heart Rate Estimation Method Based on Temporal and Spectral Sparseness of Heartbeat Signal

by

Chen Ye

Submitted to the Graduate School of Science and Technology
in partial fulfillment of the requirements for the degree of

Doctor of Philosophy in Engineering

at the

KEIO UNIVERSITY

August 2019



Author .....
Graduate School of Science and Technology
August 2019

Certified by .....
Tomoaki Ohtsuki
Professor, Keio University, Supervisor

Certified by .....
Iwao Sasase
Professor, Keio University, Co-supervisor

Certified by .....
Masaaki Ikehara
Professor, Keio University, Co-supervisor

Certified by .....
Tony Q.S. Quek
Professor, Singapore University of Technology and Design,
Co-supervisor

# Acknowledgments

Undertaking this PhD has been a truly life-changing experience. It would not have been possible to do without the support, guidance and encouragement of many people.

First and foremost, I would like to express my deepest and sincere gratitude to my supervisor Prof. Tomoaki Ohtsuki for the continuous support and encouragement that he gave me. Without his patience, motivation and immense knowledge, this PhD would not have been achievable. His advice was crucial to undertake new research challenges and keep persevering even in hard times when results were hard to obtain. I am deeply grateful for all the empowerment I received under his supervision that let me define my own pace.

The committee members Prof. Iwao Sasase, Prof. Masaaki Ikehara, and Prof. Tony Q.S. Quek, deserve a special mention, for their precious time and advice that helped improve the quality of this dissertation.

Assistance provided by Keio Leading Edge Laboratory (KLL) and Center of Innovation Program (COI), by offering grants to support research during my PhD study has been of a great help and deserve a special thank you.

Many thanks to all the members of Ohtsuki Laboratory, especially Dr. Kentaroh Toyoda and Dr. He Zhuang who have always been there for me, have never let me work alone and have always known how to keep me enthusiastic and looking forward to facing new challenges. Their unlimited energy is a reference for my future endeavors.

Last but not least, my family and friends gave me a great support from both mental and financial aspects. Especially, I would like to express my gratitude for my parents, Yu Ye and Jiao Chen. You all forgave me to proceed to PhD course without any complaint. Without their support, I could not finish my PhD thesis.

# Contents

# List of Figures

# List of Tables

# Abstract

Heartbeat is one of significant vital signs, and the monitoring of heart rate (HR) enables detecting the disorders of human health. In the past decades, many wearable sensors like electrocardiography (ECG) and photoplethysmography (PPG), have been applied to detect heartbeat based on information and communication technology (ICT). However, wearable devices are unsuitable in some situations, due to the additional burden on subjects. In contrast, non-contact heartbeat detection via Doppler radar realizes remote monitoring, which avoids violation of privacy and disturbance of light and ambient temperature over camera and passive infrared (PIR). In non-contact heart rate (HR) monitoring via Doppler radar, the disturbances from respiration and/or body motion is treated as a key problem in the estimation of HR.

To date, numerous methods on non-contact measurement of human's heartbeat movements have been developed. The limitations of the existing detection methods, i.e., the low robustness to motion artifacts (MA) and the extra demand for continuous parameter regulation, imply that they are not ideal candidates for heartbeat detection in a number of circumstances where subjects' movements happen frequently.

This thesis first proposes a sparse spectrum reconstruction (SSR) approach to mitigate the noise in received Doppler signal, by taking into account the spectral sparseness of heartbeat. Furthermore, a blind source separation (BSS) approach is further proposed to achieve better extraction of heartbeat in time domain, utilizing its temporal sparseness, incorporating the proposed SSR approach. The proposed non-contact heartbeat detection method is both provided with stability and convenience of use. In addition, the HR estimation method using our proposal delivers more satisfactory precision and robustness over other existing methods, which is demonstrated through measurements under various conditions, gaining both smallest absolute errors of HR estimation for sitting still and typewriting.

In Chapter 1, the background of HR estimation using Doppler radar, some typical existing approaches, and the two proposed approaches of SSR and BSS, are introduced in turn.

In Chapter 2, as related works to our proposal, the existing methods for heartbeat detection and their limitations, and motivations are elaborated.

In Chapter 3, the stochastic gradient approach is applied to reconstruct a high-resolution spectrum of heartbeat, by proposing the zero-attracting sign least-mean-square (ZA-SLMS) algorithm. To correct the quantized gradient of cost function, and penalize the sparse constraint on the updating spectrum, more accurate heartbeat spectrum is reconstructed. To better adapt to the noises with different strengths caused by subjects' movements, an adaptive regularization parameter (AREPA) is introduced in the ZA-SLMS algorithm as an improved variant, which can adaptively regulate the proportion between gradient correction and sparse penalty. Moreover, in view of the stability of location of spectral peak associated with HR when the size of time window slightly changes, a time-window-variation (TWV) technique is further incorporated in the improved ZA-SLMS (IZA-SLMS) algorithm, for more stable HR estimation.

In Chapter 4, the proposed BSS decomposes the spectrogram of mixture signal into original sources including heartbeat using non-negative matrix factorization (NMF) algorithms, through learning the complete basis spectra (BS) by a hierarchical clustering. Moreover, to exploit the temporal sparseness of heartbeat component, two variants of NMF algorithms with sparseness constraints are applied as well, namely sparse NMF (SPNMF) and weighted sparse NMF (WSPNMF). In particular, over the uniform sparseness constraint of SPNMF algorithm, the WSPNMF algorithm further penalizes weighted sparseness constraints on each updating estimated signal, focusing on the evident difference of sparseness between heartbeat and other sources in time domain.

In Chapter 5, our proposal on HR estimation via Doppler radar, i.e., the SSR approach acting on heartbeat spectrum reconstruction and the BSS approach functioning in extraction of heartbeat component, is concluded. Finally, some possible research directions are discussed based on specific applications.

# Chapter 1

# Introduction

Electronic health (e-Health) will have enormous applications in future healthcare systems. A typical case is the telemedicine service and assisted living for elderly people in an aging society [1]. In particular, heartbeat is one of significant vital signs, and the monitoring of heart rate (HR) enables detecting the disorders of human health [2–4]. Wearable monitoring devices (attached to chest, wrist, fingertip, or earlobe) require the embedded electrodes to directly contact wearers' skin, e.g., electrocardiography (ECG) sensor [5] and photoplethysmography (PPG) sensor [6], which limits people's daily actions due to the additional burden [1,4]. An example of ECG sensor is shown in Fig. 1-1.

## 1.1 HR Estimation via Doppler radar

In contrast, contact-free HR measurement has been increasingly drawing attentions. The contact-free devices for HR measurement typically fall into several main categories, i.e., camera, passive infrared (PIR), and radar sensor [2]. Even though imaging-based camera and temperature-based PIR achieve the remote detection of heartbeat, subjects' privacy may be violated in some circumstances, e.g., bathroom. Also, the availability of detection by camera is limited by light and obstacles, and the effect of RIP is easily influenced by temperature [2, 7]. Instead, the non-contact detection via Doppler radar is of several evident advantages, e.g., availability to the


Figure 1-1: ECG sensor [https://www.koenenco.nl/wp-content/uploads/2015/08/JM-01-webiste-04.jpg]

patients with burn or skin disease, long-period monitoring owing to flexible range, and good penetrability of electromagnetic wave that can pass through clothing [2, 3, 7]. A continuous wave (CW) Doppler radar is one of the famous types of radar systems in this filed due to its simplicity and high sensitivity [7], which is shown in Fig. 1-2. In the last decades, Doppler radar-used heartbeat detection has been researched in many fields, covering medical science and healthcare, etc [2, 3]. Specifically, chronic heart failure patient study [8], sudden infant death syndrome (SIDS) monitoring [9], monitoring of driver's condition [10], seniors and children monitoring during sleep [11], and life sensing after earthquake [12], are typical applications of this technology.

However, since radar signals are less sensitive than ECG or PPG, and the chest-wall variation induced by heartbeat is generally smaller than that by respiration, the interference of respiration and/or subjects' movements forms a main challenge in the HR estimation with Doppler radar [4, 13, 14].

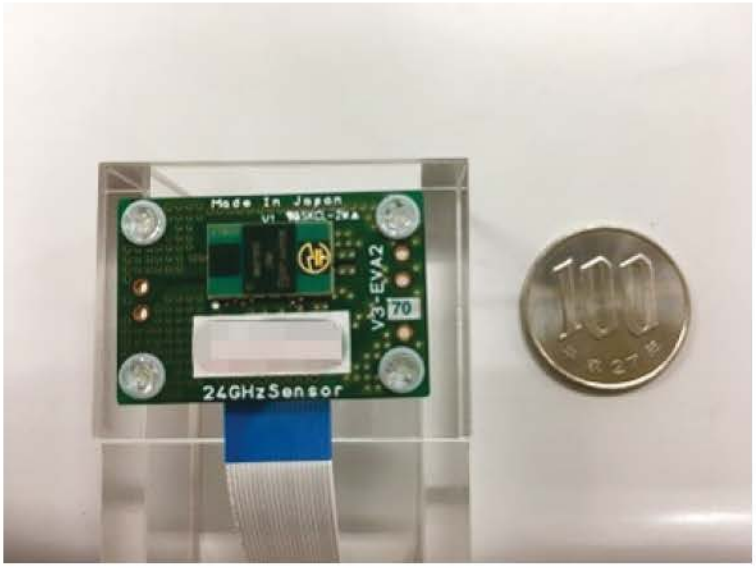


Figure 1-2: CW Doppler radar

## 1.2 CW Doppler radar

### 1.2.1 Signal Transmission and Reception

The basic theory of Doppler radar detection for vital signs is remotely capturing and analyzing the phase variation, reflected by human physiological motion. Fig. 1-3 shows a typical radar front-end structure that functions to HR measurement, with signal flow. The unmodulated signal transmitted from transmitter (Tx) can be expressed as

$$T(t) = \cos\left[2\pi f t + \Psi(t)\right], \tag{1.1}$$

where $f$, $t$, and $\Psi(t)$ respectively represent carrier frequency (24 GHz), transit time, and initial phase. After the transmission through a distance $d_0$, the time-varying chest-wall displacement $x(t)$ of a target due to breathing and heartbeat changes $T(t)$, and the signal received at receiver (Rx) becomes

$$R(t) \ll \cos\Big]2\pi f t \quad \frac{4\pi d_0}{\lambda} \quad \frac{4\pi x(t)}{\lambda} + \Psi\Big)t \quad \frac{2d_0}{c}\Big[\Big\{, \tag{1.2}$$

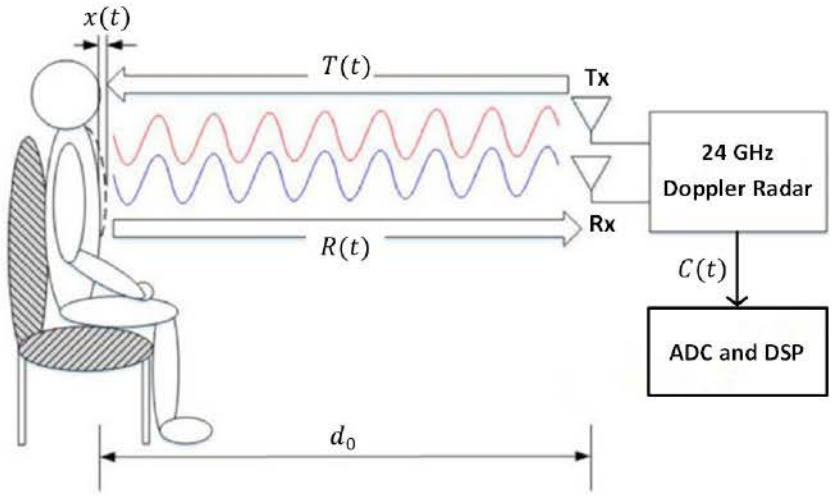


Figure 1-3: Typical structure of Doppler radar heartbeat detection system

omitting the amplitude and extra noise. $\lambda$ and $c$ denote wavelength and velocity of electromagnetic wave, respectively.

For a single-tone periodic movement, $x(t) = m \sin 2\pi f_m t$ where $f_m$ and $m$ are frequency and amplitude of a subject's movement, respectively. Since the periodic cardiopulmonary movement is more complex, it can be decomposed into single-tone signals, i.e., $x_h(t) = m_h \sin 2\pi f_h t$ induced by motion information of heartbeat, and $x_r(t) = m_r \sin 2\pi f_r t$ by respiration. In the HR measurement, the objective is to detect the HR denoted as $f_h$, by processing baseband signals that will be depicted in the following subsection.

### 1.2.2 Generation of Baseband Signals

In CW Doppler radar, two main operations are executed to $R(t)$, namely down-conversion with reference signal (i.e., $T(t)$) and quadrature mixing. The resultant baseband signals consisting of in-phase signal $B_I(t)$ and quadrature signal $B_Q(t)$ are

$$B_I(t) = \cos\left]\frac{4\pi x(t)}{\lambda} + \theta + \Delta\Psi(t)\right\{, \tag{1.3}$$

$$B_Q(t) = \sin\left]\frac{4\pi x(t)}{\lambda} + \theta + \Delta\Psi(t)\right\{, \tag{1.4}$$

where $\theta = (4\pi d_0)/\lambda$ is the phase shift determined by the distance $d_0$ between the radar and the target. $\Delta\Psi(t) = \Psi(t) \quad \Psi(t \quad 2d_0/c)$ is the residual phase noise. In addition, to remove the possible direct current (DC) offset mainly due to clutter reflections [2], a clutter calibration is implemented to adaptively adjust the mean-amplitude of baseband signals to zero. In general, the two quadrature baseband signals are combined as a complex signal:

$$C(t) = B_I(t) + iB_Q(t), \tag{1.5}$$

followed by analog-to-digital conversion (ADC) and digital signal processing (DSP), to analyse digitalized $C(t)$.

## 1.3 Existing Approaches

Along with the growing interests in non-contact HR monitoring, numerous detection approaches have been developed [14–18]. In general, existing approaches mainly fall into frequency domain and/or time domain as follows:

(1) Frequency domain: Fast Fourier transform (FFT) [14, 16, 19–22] and continuous wavelet transform (CWT) [4, 15, 23–26].

(2) Time domain: Adaptive noise cancelation (ANC) [27], arctangent (AT) demodulation [17], and ensemble empirical mode decomposition (EEMD) [18].

The approaches in (1) are usual frequency domain transform techniques, which are called conventional ones of spectrum reconstruction in this thesis. In contrast, the approaches in (2) typically rely on the processing in time domain. The existing methods of heartbeat detection using afore-mentioned approaches, have been shown to be able to effectively realize remote HR estimation, in relatively ideal conditions where

subjects' movements rarely occur, e.g., sitting still [4,9,16], sleep monitoring, and infant monitoring [28,29]. Meanwhile, when a subject is relatively static, the heart rate variability (HRV) is not obvious along with time, differing from the case when body motion exists [30,31]. In fact, a degree of body motion should be considered in many practical applications, such as, HR monitoring to office workers or drivers [15]. However, most existing detection methods cannot deal with the motion artifacts (MA), i.e., the noise interference caused by body motion, resulting in a significant performance degradation [4,9]. Also, in the presence of body motion, a real-time parameter regulation for some existing approaches is indispensable due to the observable HRV. A typical case is the selection of scale factor for the CWT-based methods [15, 25], which will be elaborated in Section 2.1. Furthermore, typical state-of-the-art methods on HR estimation using various approaches, and their limitations are reviewed in Chapter 2.

## 1.4 Proposed Approaches

In view of the limitations of existing approaches and motivations in non-invasive heartbeat detection, we first proposes a frequency domain-based sparse spectrum reconstruction (SSR) approach functioning in reconstructing heartbeat spectrum, for more reliable HR estimation considering MA. Then, to improve the noise elimination in time domain, an unsupervised blind source separation (BSS) approach is further proposed inheriting the basic framework of HR measurement with the proposed SSR, bringing about performance improvement.

### 1.4.1 SSR in Frequency Domain

Considering the evident advantages of ZA-SLMS algorithm for sparse signal reconstruction, i.e., superior performance and robustness, we first apply it to the SSR part in our proposed method of heartbeat detection. In particular, the proposed ZA-SLMS algorithm can suppress well the interference originated from respiration and/or moderate body motion, e.g., typewriting. As a preliminary work, we have shown the

validity of the ZA-SLMS algorithm in [40].

To the sparse adaptive algorithms, including our proposed ZA-SLMS algorithm, the regularization parameter (REPA) plays a key role to balance the proportion between gradient correction and sparse penalty, which should be properly chosen to guarantee satisfactory performance [44]. As mentioned above, MA often overwhelms the heartbeat signal due to its weakness, which directly associates with the variation of amplitude of radar signal [30, 31, 41]. In addition, the diversity of noise strengths based on different kinds of body motion is distinct [9,30,31,41]. However, the constant REPA probably determines an improper weight of sparse penalty on updating spectrum, against different subjects' activities. Motivated by the fact that the amplitude variation of received radar signal relates with the strength of interference by body motion, a novel adaptive REPA (AREPA) is introduced by further proposing an improved ZA-SLMS (IZA-SLMS) algorithm. The IZA-SLMS algorithm can adaptively regulate the sparse penalty to a proper proportion based on the standard deviation of radar signal, to obtain more accurate HR estimation over the ZA-SLMS algorithm, facing various subjects' activities.

In another aspect, by incorporating the conventional FFT [14] or CWT [26], a practical HR acquisition technique termed time-window-variation (TWV) applied in non-contact heartbeat detection has gained popularity. Unlike the usage of the single time window adopted in most existing methods, the TWV technique reconstructs spectra by the samples of received signal in multiple time windows with varying lengths, then the highest peak on the combined spectrum is selected within a normal HR range [14, 26]. Although the TWV with FFT or CWT, reduces the measurement errors of HR over usual single window, it has not been attempted to incorporate more advanced method of spectrum reconstruction, e.g., the SSR. In this thesis, to further enhance the stability of HR estimation, TWV is applied to SSR by the improved IZA-SLMS algorithm.

### 1.4.2 BSS in Time Domain

Moreover, the other main purpose of this thesis is to present an easy-to-use, compact, and accurate unsupervised BSS approach based on non-negative matrix factorization (NMF) structure [45–48], to robustly demix Doppler signal into individual sources, i.e., heartbeat, respiration, and body motion, combining with SSR for HR estimation. The structure of NMF is fairly simple that merely needs observation signal of single channel, bringing about high computational efficiency compared with typical emerging learning methods, e.g., deep clustering [49]. In addition, besides the standard NMF algorithm [45, 46], we further propose two improved NMF algorithms with sparseness constraint, i.e., the sparse NMF (SPNMF) [50] and the weighted sparse NMF (WSPNMF), to exploit the inherent sparsity of heartbeat in time domain.

In BSS, the learning of a separation matrix that we name as basis spectra (BS), is one of important tasks for demixing observation signal. In view of the time-varying feature of vital signs that includes the variability of HR induced by physical or mental conditions [30], the training data for supervised learning of BS (heartbeat-only signal) hardly satisfy a continuous monitoring, specifically for infants or patients who have troubles in self-control [51] or sleeping people [52]. In view of the fact, we propose an unsupervised manner-based BSS, consisting of three steps: two progressive clusterings and a complete learning on BS. *1) First Clustering:* In this step, the short-time Fourier transform (STFT)-based magnitude spectrogram $\mathbf{X}$ is first obtained by the received radar signal in a small batch, which is equal to the size of a time window in our method. Then, the NMF algorithm decomposes the non-negative part of $\mathbf{X}$ (denoted by $\mathbf{X}_+$) into a set of underlying basis vectors, acting on the reconstruction of eventual BS. *2) Second Clustering:* Unlike the direct factorization in the first clustering, the prior knowledge of source signals, i.e., the number and components, should be known beforehand for the second clustering. Although it is possible to neglect movements to a static examinee through cardiopulmonary sounds obtained by attached auscultation [51], even tiny body motions evidently vary Doppler signal [40], which is also treated as an individual source to motionless state (e.g., sitting still)

in our proposal, besides heartbeat and respiration. On the assumption of $I = 3$ sources, the specific region of $\mathbf{X}_+$ concentrating dominant heartbeat and respiration with periodicity is chosen as decomposition target by NMF algorithms, for acquiring $I$ reference BS (RBS). *3) Complete BS Learning:* To learn a complete BS in each time window, RBS are dynamically updated by analyzing the maximum similarity between the respective basis vectors, obtained in the first and second clusterings. Based on the determined complete BS, the observation matrix (i.e., $\mathbf{X}_+$) is factorized to estimate sources, and the interested heartbeat can be extracted through observing spectrum magnitude. A part of results of the proposed BSS approach have been published in [53], as a preliminary work.

It is easy to find that temporal heartbeat signal has prominent sparsity, due to the generation mechanism in ventricles, namely instantaneous impulsive motions happen during the systolic phase [13]. In the specific application of BSS for heartbeat source (e.g., heart sound), the main factorization algorithm is limited to standard NMF yet [51, 54], which may not reach satisfactory decomposition with the sole non-negativity penalty. Inspired by the fact, we further implement sparseness penalties on the estimated signals in the both clusterings to improve local representations, by applying SPNMF algorithm and WSPNMF algorithm. Due to the obvious temporal sparsity of heartbeat, it is comprehensible that holistic sources also have certain sparsity, and the SPNMF algorithm imposes a uniform sparseness constraint during mixture decomposition [50]. In addition, we apply flexibly the proportions of sparsity penalty of the SPNMF algorithm on each estimated signal, through adaptively sensing periodicity of updating signals, naturally obtaining a modified SPNMF algorithm termed WSPNMF in this thesis.

## 1.5 Contributions

In contrast to most existing non-invasive HR estimation methods that can not well balance convenience of use and anti-noising to movements, our proposal achieves robust HR measurement on the compromise of wide practicability, exploiting the

temporal and spectral sparseness of heartbeat source. In particular, over usual BSS, our proposed BSS has three advantages: (i) Clustering-induced unsupervised manner; (ii) Compact demixing architecture; and (iii) Merely requiring single-channel input data.

Through the experiments on five subjects, we evaluated the effects of the two proposed approaches, i.e., SSR and BBS. The HR measurement methods by our proposal outperform some existing methods presented recently, both against motionless and active conditions. In particular, in the activity of typewriting, the proposed methods using IZA-SLMS with TWV and the one using WSPNMF, respectively acquired the most precise estimations with average errors of 3.79 beats per minute (BPM) and 3.35 BPM.

## 1.6 Outline of Dissertation

The remainder of this thesis is organized as follows.

- Chapter 2 reviews the HR estimation-aimed existing methods using various approaches in frequency domain or time domain, and indicates their limitations and motivations.
- Chapter 3 elaborates the proposed SSR approach in frequency domain based on the corresponding framework, with performance evaluation by experiments.
- Chapter 4 further elaborates the proposed BSS approach in time domain based on the enhanced framework, with performance evaluation by experiments.
- Chapter 5 concludes this thesis, and indicates the possible research direction in future.

For better understanding this dissertation, the organization and the relation among key chapters are shown in Figs. 1-4 and 1-5, respectively. Also, Tables 1.1 and 1.2 list the limitations of existing approaches based on frequency domain or time domain, and the contributions of Chapters 3 and 4, respectively.

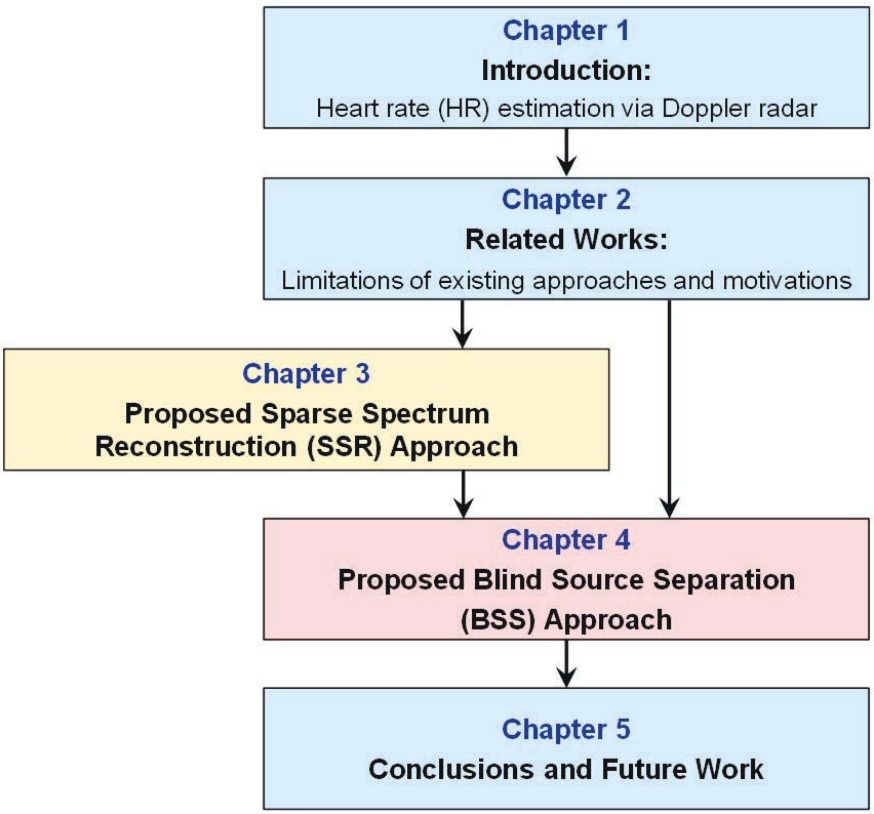


Figure 1-4: The organization of this dissertation

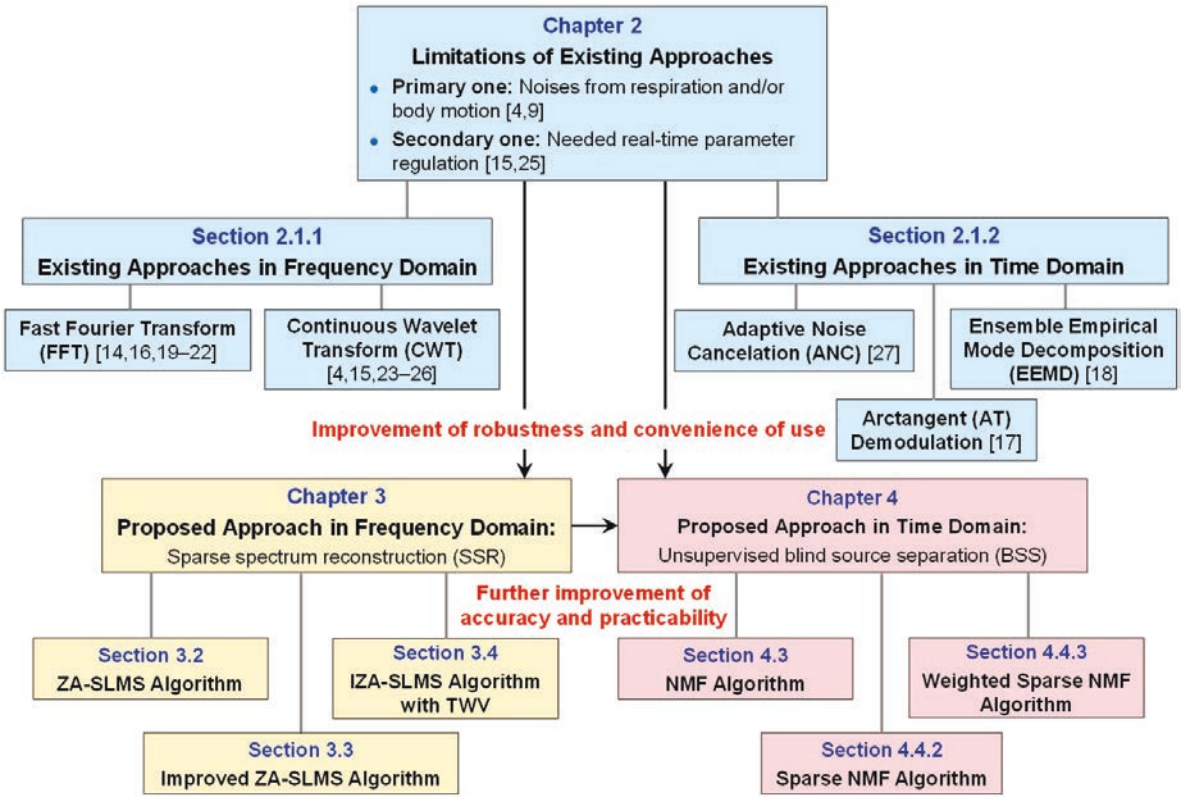


Figure 1-5: The relation among key chapters

Table 1.1: Limitations of existing frequency-based approaches and contributions of Chapter 3

| | |
|---|---|
| **Research Problem** | • The interference of respiration and/or subjects' movements forms a main challenge in the HR estimation with Doppler radar [4, 13, 14]. |
| **Limitations of Existing Approaches** | • Fast Fourier transform (FFT) [14, 16, 19–22]: An incorrect heartbeat detection probably occurs due to body motion, resulting in an evident degradation of performance.<br>• Continuous wavelet transform (CWT) [4, 15, 23–26]: For continuous measurement of HR, a real-time regulation of scale factor associated with HR is necessary. |
| **Proposed Approach** | • A robust heartbeat detection method is proposed considering the sparseness of heartbeat spectrum, through enhancing sparse spectrum reconstruction (SSR) by applying the ZA-SLMS algorithm.<br>• An improved ZA-SLMS algorithm and the incorporation of TWV technique are further proposed. |
| **Improvements** | • Better robustness to noises originated from respiration and body motion.<br>• The usage becomes more convenient, avoiding real-time regulations of parameters. |

Table 1.2: Limitations of existing time-based approaches and contributions of Chapter 4

| | |
|---|---|
| **Research Problem** | • The interference of respiration and/or subjects' movements forms a main challenge in the HR estimation with Doppler radar [4, 13, 14]. |
| **Limitations of Existing Approaches** | • Adaptive noise cancelation (ANC) [27]: The respiration-only signal as reference is difficultly acquired, and multiple antenna structures may be infeasible in some scenarios.<br>• Combination of arctangent (AT) demodulation [17] and ensemble empirical mode decomposition (EEMD) [18]: The method presented in [9] is clarified to difficultly deal with body motion, out of specific treatment such as dynamic motion compensation.<br>• Singular spectrum analysis (SSA) [40]: The SSA-based abstraction of heartbeat component heavily depends on spectrum distribution of other sources, i.e., respiration and movements. |
| **Proposed Approach** | • An unsupervised blind source separation (BSS) based on non-negative matrix factorization (NMF) structure, is further proposed to abstract heartbeat component, based on the proposed method [40] in Chapter 2.<br>• By exploiting the temporal sparseness of heartbeat signal, two sparse versions of NMF algorithms named SPNMF and WSPNMF are proposed as well. |
| **Improvements** | • Improved accuracy of HR estimation owing to better heartbeat abstraction.<br>• Compact structure of sources separation by NMF algorithms, without training phase. |

# Chapter 2

# Related Works

In this chapter, some typical approaches in state-of-the-art HR estimation methods are first reviewed. Then, the limitations of existing approaches, and the motivations including the prominent temporal and spectral sparseness of heartbeat are depicted, respectively.

## 2.1 Existing Methods for HR Estimation

To date, numerous methods on non-contact measurement of human's heartbeat movements have been developed, which apply various approaches of signal processing falling into either frequency domain [4, 14, 16, 23, 24, 26, 40] or time domain [4, 9, 13, 27, 40].

### 2.1.1 Frequency Domain-Based Approaches

As a conventional frequency domain approach, FFT can divide the sampled data into each frequency component, which separates heartbeat and noises, and it has been widely applied in HR measurement [14, 16, 19–22]. In [14], FFT is first combined with the TWV technique, which can fast acquire HR with smaller errors. In [16], the spectrogram of radar signal is calculated by the extended short-time Fourier transform (STFT), then the R-R intervals (RRIs) can be observed by the period of neighboring

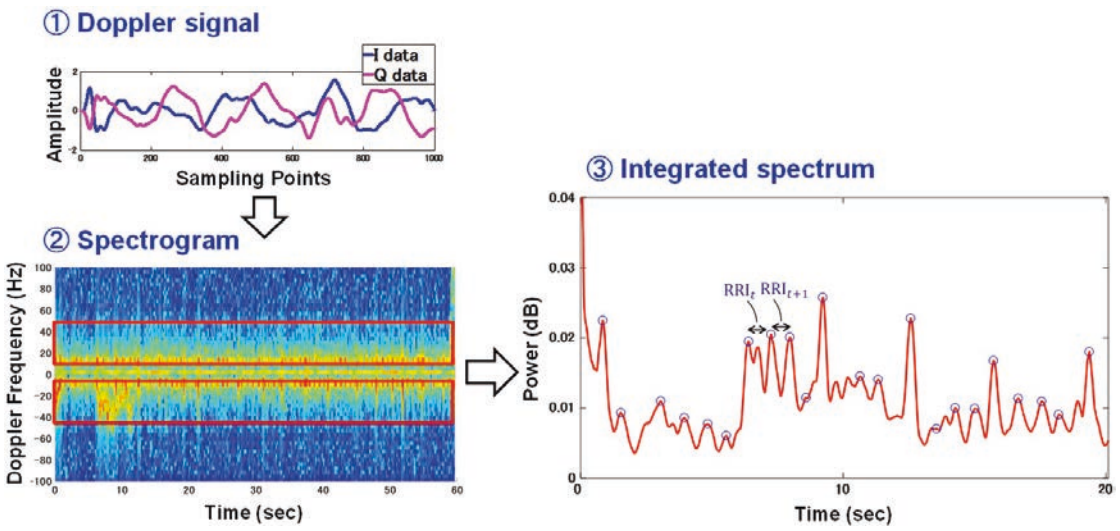


Figure 2-1: The basic procedure of Spectrogram method [16]

peaks on the integrated spectrum, which is accumulated from the spectrogram in a normal HR range. Fig. 2-1 shows the procedure of Spectrogram method for better understanding. The effectiveness of the mentioned FFT-based methods have been validated, when a few movements from subjects arise, such as usual sitting still. However, Doppler radar signal is vulnerable to MA, which will bring incorrect RRI measurements in the presence of body motion, accompanying markedly increased errors [4, 9].

Unlike FFT, CWT has more flexible time-frequency resolution, which can increase the resolution of low frequency range adapting to HR extraction. In the CWT-based detection methods [4, 15, 23–26], to realize that the resultant wavelet coefficients can correspond with heartbeat, the mother wavelet should have same or close frequency to HR, which is determined by the key scale factor. To choose a proper scale factor, some selection methods have been proposed [15,25]. In particular, Mogi *et al.* [15] presented an adaptive scale factor selection method, namely, to search the wavelet coefficients whose peaks count is equal to that of the voltage data generated from radar signal, then the scale factor corresponding to the interested wavelet coefficients is chosen. For intuitive illustration, the basic procedure of adaptive scale factor selection method is shown in Fig. 2-2. For the usage of CWT-based methods, the scale factor is

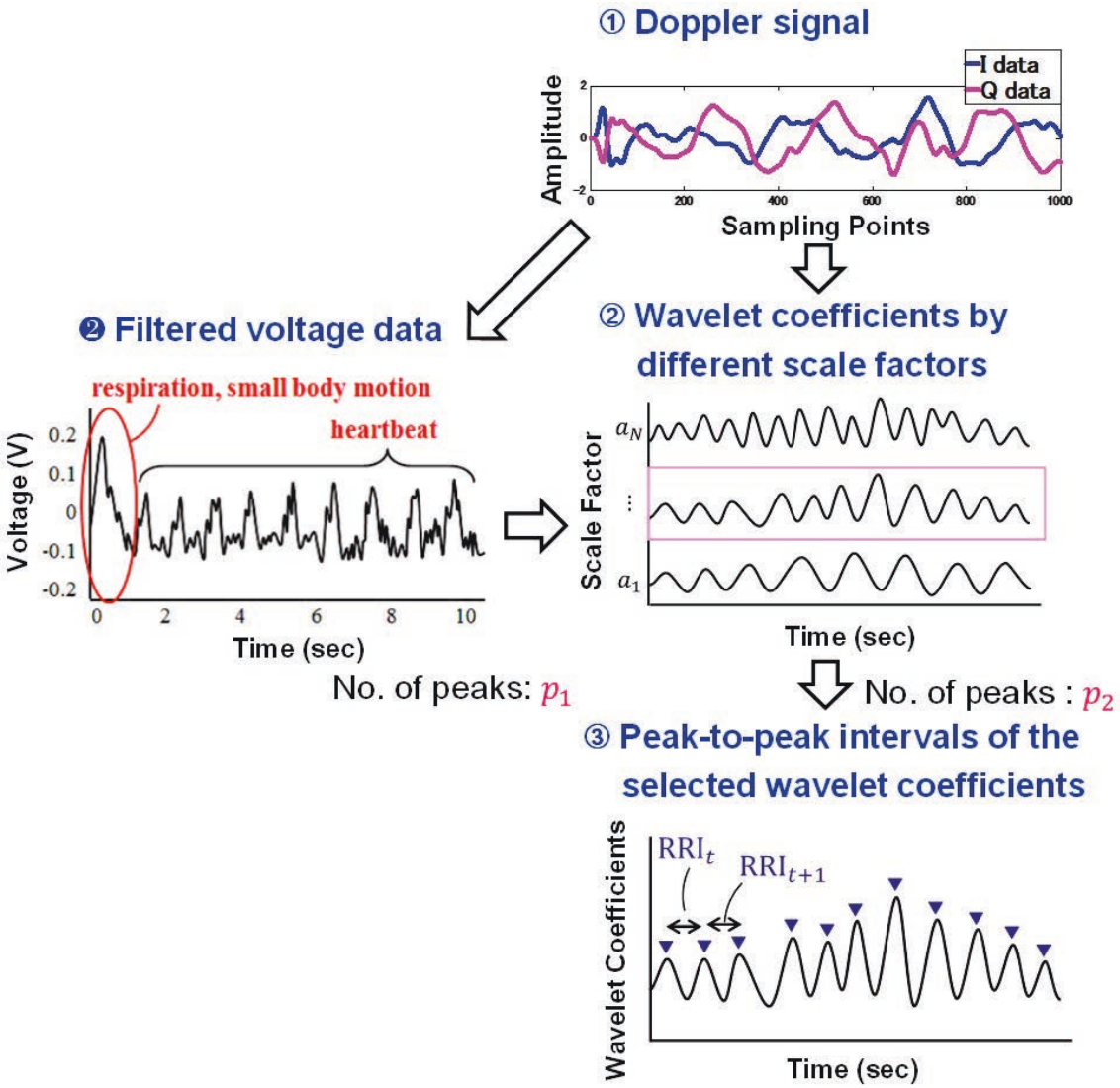


Figure 2-2: The basic procedure of adaptive scale factor selection method [15]

typically constant, also, an improper choice or change probably lead to an inaccurate heartbeat detection. However, HR varies along with time, and its variation will be more significant when body motion occurs [30]. Correspondingly, a real-time and appropriate selection of scale factor is desired to reliable HR measurement, which may be difficult in most applications [16, 40].

Meanwhile, some literatures have reported that MA components can be recognized by acceleration data in wearable devices [30, 31, 41]. Specifically, Zhang *et al.* [30] proposed a stable framework termed TROIKA. The TROIKA mainly consists

of signal decomposition and SSR, which realizes high estimation accuracy against strong MA, by PPG signal and acceleration data. In the signal decomposition part, the interference from subjects' movement can be removed relying on acceleration data, then a relatively cleansed PPG signal can be obtained for SSR. Unfortunately, since few studies proved that acceleration sensor can be effectively utilized in remote HR monitoring, the removal of MA is a challenging task. Furthermore, unlike on-body heartbeat detection, the respiration movement is another main noise source of the non-contact way. When the TROIKA framework is assumed to be applied in the HR measurement with Doppler radar, the residual noises of respiration and body motion after signal decomposition, may bring serious influence on the reconstruction of heartbeat spectrum. In [30], a regularized focal under-determined system solver (FOCUSS) algorithm [37] considering multiple-measurement-vectors, termed RM-FOCUSS [38], has been used for SSR in TROIKA, due to the robustness to the basis matrices with highly correlated columns. However, the FOCUSS-type algorithms are sensitive to additive noise, and probably fail to reconstruct the interested nonzero coefficients [37,38]. In view of the misfits of RM-FOCUSS algorithm for SSR by Doppler radar signal, an anti-noise SSR algorithm is needed.

### 2.1.2 Time Domain-Based Approaches

So far, plenty of time domain approaches used for remotely detecting HR have been studied, which mainly focus on the probe of heartbeat periodicity by signal amplitudes [4, 13], or the extraction of heartbeat component by noise elimination [9, 27, 40]. In [4], using Doppler signal, the peaks in autocorrelation function of calculated wavelet coefficients are selected to estimate R-R intervals (RRIs), by means of the peak ratio of autocorrelation. However, when an improper time-frequency resolution is chosen in CWT, incorrect selection of peaks of autocorrelation easily occurs. In [13], radar signal with inherent sinusoidal shape is trained by Guassian pulse, to represent a more realistic pulsed characteristic of heartbeat. However, the application of Guassian pulse training is only bounded to the examinees staying as basically motionless. Lu *et al.* applied the ANC to suppress the interference of respiration, from the reflected

signal induced by chest-wall motions [27]. However, the respiration-only signal as reference is difficultly acquired, and multiple antenna structures may be infeasible in some scenarios. Hu *et al.* combined arctangent (AT) demodulation [17] and ensemble empirical mode decomposition (EEMD) [18], to recover cardiopulmonary signals [9]. Therein, AT demodulation enables precise phase demodulation of the received signal by the ratio of quadrature baseband signals, and EEMD repeatedly cleanses heartbeat signal by decomposing the white noise-added data. However, the method presented in [9] is clarified to difficultly deal with body motion, out of specific treatment such as dynamic motion compensation. In [40], incorporating the SSR via the ZA-SLMS algorithm, a singular value decomposition (SVD)-based time series decomposition approach termed singular spectrum analysis (SSA) [42] was used to noise removal of Doppler signal, for reliable heartbeat detection. However, the selection of time series associated with heartbeat by SSA requires relatively rigorous spectrum analysis, and respiration and MA that have close or same frequencies with actual HR will disorder SSA [53]. In brief, most existing time domain de-noising means for contact-free heartbeat extraction are difficult to get rid of disturbance of movements, and most signal decompositions like EEMD and SSA have large computational burden [41], correspondingly a novel signal processing approach is desired.

## 2.2 Limitations and Motivations

The limitations of the existing detection approaches, i.e., the low robustness to MA and the extra demand for parameter regulation, imply that they are not ideal candidates for heartbeat detection in a number of circumstances where subjects' movements happen frequently. As such, a more reliable and practical non-contact heartbeat detection method is of urgent need for applications to more general scenarios.

In fact, some literatures have clarified that the sparse spectrum reconstruction (SSR) approach can acquire higher spectral resolution than the conventional FFT and CWT [30, 32], which inspires us to reconstruct a more accurate heartbeat spectrum by SSR. In another aspect, some robust adaptive (filtering) algorithms based on

stochastic gradient descent (SGD), have been proposed for sparse channel estimation, to effectively suppress strong noises [33]. However, the mentioned algorithms in [33] cannot directly apply in SSR, that is, to reconstruct a high-resolution of spectrum by certain sample data. Fortunately, the feasibility that sparse signal can be robustly reconstructed using compressed data, by adaptive algorithms combining sparse penalty, has been manifested in [34]. Also, the sparse adaptive algorithms have been demonstrated to outperform most typical algorithms for sparse signal reconstruction [34–38]. Specifically, an improved sparse adaptive algorithm termed zero-attracting sign least-mean-square (ZA-SLMS) realizes robustly the reconstruction of sparse signal, by restricting the scale of gradient correction [39]. In this thesis, the ZA-SLMS algorithm and its variants will be first applied to accomplish SSR of heartbeat component.

Furthermore, though SSR overcomes many limitations of conventional spectrum reconstrction by utilizing the spectral sparsity of heartbeat, which greatly increases the resolution of reconstructed spectra and simplifies the parameter settings [30,32,34, 40], the SSR is susceptible to the noises remained in received radar signal [40]. Even if some improved SSR algorithms have been presented, such as the ZA-SLMS [39], their performances still fairly rely on the previous temporal de-noising processing [40].

For the noise cancellation in time domain, signal decomposition has been widely used in heartbeat detection methods, specifically, singular spectrum analysis (SSA) is proved as a powerful approach to decompose signal due to the flexibility of operation [30, 40, 41]. The basic idea of SSA is to reconstruct multiple time series, using the singular values calculated by the mapped matrix from the considered signal [42]. In SSA-based HR estimations, the selection of noise-free time series severely relies on spectral interpretation (generally by Periodogram), and noise recognition by aided knowledge [30, 41]. For instance, using Periodogram to calculate the spectra of each time series from PPG signal and acceleration data, the MA component is recognized and cancelled by removing the dominant magnitudes induced by acceleration data, in [30, 41]. Otherwise, the representative problem existing widely in algorithms of spectrum reconstruction (e.g., Periodogram algorithm via FFT [43]), namely the leakage effect, makes frequency components inseparable [30,43]. Through treating the

leakage effect by spectrum subtraction, the heartbeat-induced spectral peaks become prominent, which enables the precise extraction of the time series reflecting HR.

In contrast to the invasive detection, generally, acceleration sensor can not work well for remotely measuring HR. Lacking of a feasible identification of noises in SSA, the interference of respiration and MA becomes a challenging issue in the non-invasive detection using Doppler radar signal [40]. More concretely, the nearby spectral amplitudes corresponding to respiration and/or movements weaken even overwhelm the spectral peaks associated with HR, resulting in a noise-contaminated heartbeat signal, i.e., the targeted time series reconstructed by SSA. The obvious residual noises easily restrain the effects of following frequency domain processings, due to the unsolved leakage effect. In addition, the serious problem also limits the exploitation of spectral sparsity of heartbeat in the usage of superior SSR, which has been presented as an open question in [40]. To extract relatively cleansed heartbeat component for Doppler radar detection, an alternative of SSA is urgently needed.

### 2.2.1 Sparseness of Heartbeat Signal

Fig. 2-3(a) intuitively illustrates a segment of heartbeat signal recorded by ECG sensor in time domain, where the impluse characteristic of signal exhibits the evident temporal sparseness. Also, the reconstructed spectrum by the heartbeat signal is shown in Fig. 2-3(b), the spectral sparseness of heartbeat signal can be easily found by the dominant power peak, and the other magnitudes are close to zero. In contrast, most vital signs do not have obvious sparseness as heartbeat signal, such as respiration or blink signals. Inspired by the remarkable sparseness both in time domain and frequency domain, we improve the proposed approaches of BSS and SSR by penalizing sparse constraint, which will be elaborated in the following context.

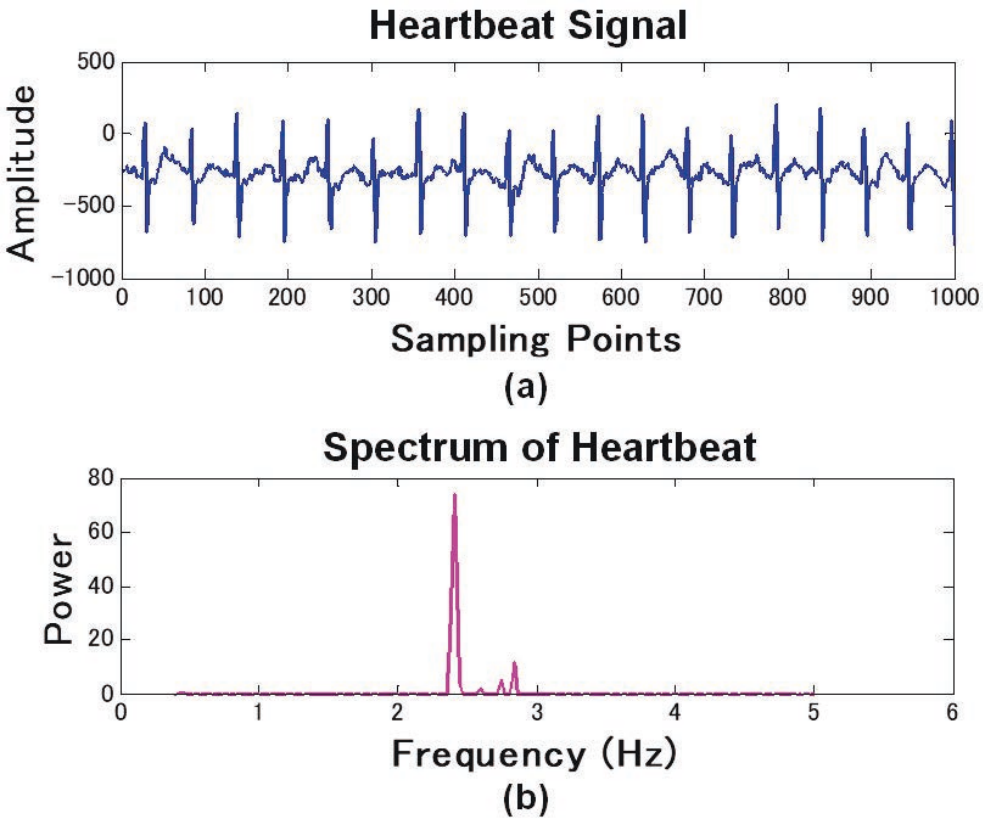


Figure 2-3: A segment of heartbeat singal and its spectrum with sparseness

# Chapter 3

# Proposed SSR Approach

In this chapter, first, an applied HR measurement framework incorporating the proposed SSR approach is described. Then, three proposed SSR algorithms are depicted, successively. Finally, the experimental results by multiple metrics are provided.

## 3.1 Framework of HR Measurement

To realize accurate HR estimation with Doppler radar during subjects' movement, a stable framework is proposed as shown in Fig. 3-1. Raw radar signal is processed by pre-processing, signal decomposition, and temporal difference for noise elimination. SSR yields a high-resolution spectrum reconstruction, following a binary decision that decides whether TWV is adopted. Next, the spectrum peak tracking would find the spectral peak corresponding to HR. For better understanding the superiority of the proposed method, namely the robustness to MA, the ZA-SLMS algorithm and its improved variant acting on SSR, and the introduction of the TWV technique are elaborated.

In this thesis, the Doppler signal $C(t)$ in each time window of $T_0 = 8$ s is input to the proposed framework for HR estimation. Note that 8 s is an appropriate size of time window for heartbeat detection that has been adopted in [30, 41], considering that relatively large $T_0$ can achieve a high spectrum resolution on the compromise of prompt observation of HRV. Each signal processing part is depicted in order, as

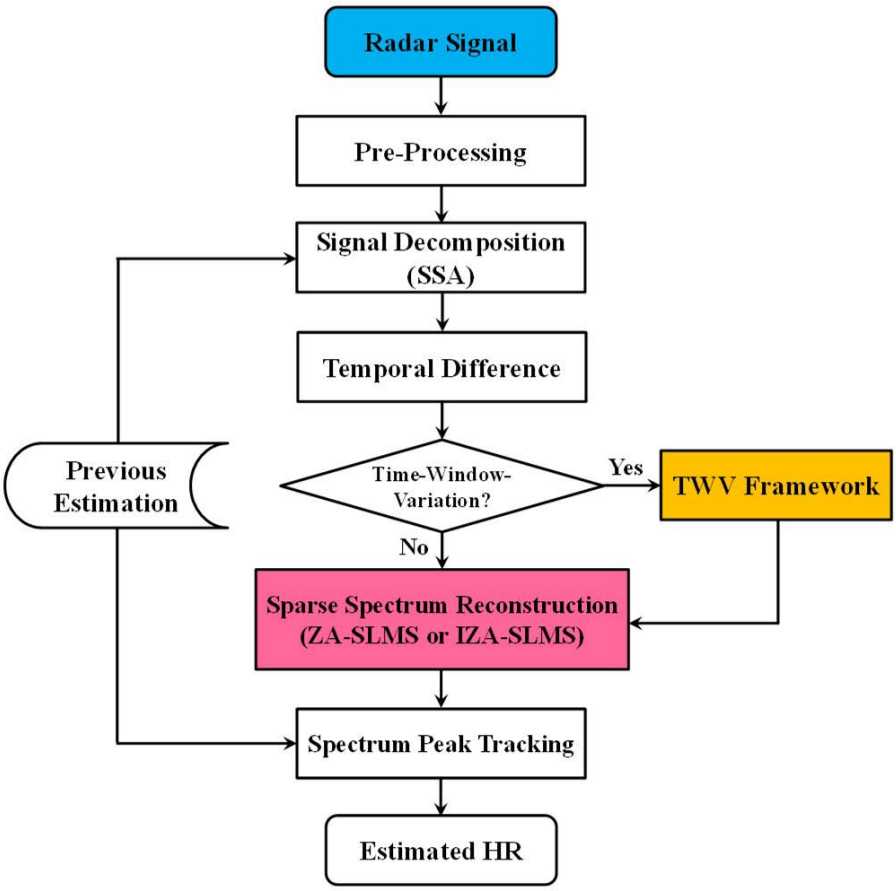


Figure 3-1: The flowchart of HR measurement framework, incorporating our proposed SSR approach

follows.

### 3.1.1 Pre-Processing

Pre-processing consists of down-sampling and bandpass filtering. To reduce redundant computational burden, the radar signal is first down-sampled to 125 Hz. Besides, in view of the fact that the respiration rate typically varies within 0.1–0.3 Hz, while HR varies in a higher range of 1–3 Hz [4], a bandpass filter with cutoff frequency of 0.4–5 Hz covering the variation range of HR, is adopted to down-sampled $C(t)$. The noises including MA outside of the objective frequency band can be filtered, also, the sparsity of spectrum becomes more dominant.

### 3.1.2 Signal Decomposition

Followed by the pre-processing of signal, the singular spectrum analysis (SSA) [42,55] is used to extract heartbeat components, in the signal decomposition part. First, the filtered radar signal is decomposed into some time series by singular value decomposition (SVD), then, the spectra of each time series are calculated by the Periodogram algorithm executed via FFT. Finally, through searching for the highest peak in a given HR range among the reconstructed spectra, referring to the previous estimated HR, the time series corresponding to heartbeat is obtained. Note that the interference by respiration and body motion cannot be completely eliminated, specifically, in the case that MA occurs. The residual noises motivate us to apply more robust algorithms for SSR.

### 3.1.3 Temporal Difference

In general, MA components are aperiodic, while respiration and heartbeat are approximately periodic [30]. In order to promote the periodic fluctuations of the de-noised radar signal, the temporal difference is operated between signal decomposition and SSA. To the time series presenting heartbeat of the length $M = 1000$, which is output by SSA, i.e.,

$$\mathbf{y} = [y_1, y_2, \ldots, y_M]^{\mathrm{T}}, \tag{3.1}$$

where $(\cdot)^{\mathrm{T}}$ denotes the transpose, its first-order difference is defined as

$$\mathbf{y}' = [y_2 \quad y_1, y_3 \quad y_2, \ldots, y_M \quad y_{M-1}]^{\mathrm{T}}. \tag{3.2}$$

To coincide with the count of samples in $\mathbf{y}$, i.e., $M$, $\mathbf{y}'$ is approximated by

$$\mathbf{y}' = ]0, \mathbf{y}'^{\mathrm{T}}(^{\mathrm{T}}. \tag{3.3}$$

By temporally differentiating the de-noised radar signal, the random spectral power induced by MA can be reduced [30].

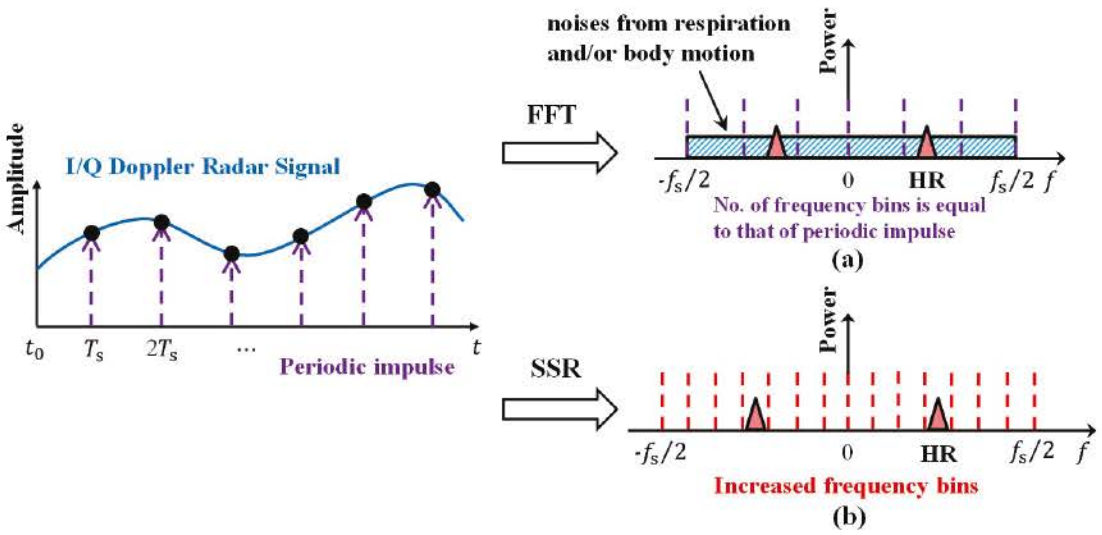


Figure 3-2: An comparison of spectrum reconstruction methods by Doppler radar signal, where $T_s$ and $f_s$ respectively denote sampling period and frequency. (a) Conventional FFT. (b) Proposed SSR

### 3.1.4 SSR (with TWV)

SSR [32, 35, 36] overcomes the traditional Nyquist sampling limit, which enables the acquisition of high-resolution spectrum, by developing the sparsity of signal. The main task of SSR is to reconstruct the spectrum of interest, i.e., the heartbeat spectrum in this study, based on an under-determined linear equation as follows,

$$\mathbf{y}' = \mathbf{\Phi s} + \mathbf{v}. \tag{3.4}$$

Here $\mathbf{s}$ is an unknown solution of original heartbeat spectrum with inherent sparsity, $\|s_k\|^2$, $k$ / $\}1, \times\times\times, N|$ is the corresponding heartbeat spectrum of length $N = 4096$ ($M \in N$), $\mathbf{v}$ represents the $M$-length residual noises of respiration and body movement, and $\mathbf{\Phi}$ / $\mathbb{C}^{M\times N}$ is a known basis matrix with the elements defined as

$$\phi_{j,k} = \mathrm{e}^{i\frac{2\pi}{N}jk},\ j = 0,\ \times\times\times,\ M \quad 1;\ k = 0,\ \times\times\times,\ N \quad 1. \tag{3.5}$$

By a proper choice of SSR algorithms, the frequency bins can be dramatically increased by limited samples of Doppler radar signal, as shown in Fig. 3-2. Owing

to the previous signal processing operations, the spectral power of noises is generally zero or close to zero, which can be further suppressed by introduced sparse constraint, and the peak associated with HR becomes more dominant.

Even though FOCUSS-type algorithms [37,38] have been demonstrated to a PPG signal to realize SSR [30, 41], the prominent spectral power of HR probably cannot be reconstructed in a low signal-to-noise power ratio (SNR). Considering that the instability of FOCUSS-type algorithms against the residual respiration noise and MA, two sparse adaptive algorithms based on SGD approach are applied in SSR part, i.e., the ZA-SLMS algorithm and its improved variant. Also, to further develop the potential of performance of the proposed algorithms, TWV technique can be incorporated by sacrificing several times of computing time, which will be separately stated later on.

### 3.1.5 Spectrum Peak Tracking

At the end, the spectral peak corresponding to HR can be estimated by a compact procedure, which is divided into following three steps:

1. Initial Setting: A variable HR search range of 20 BPM is initialized aiming to different subjects, considering that the HRV is generally within a specific range to a normal subject without big motion [16].

2. Peak Selection: Since the HRs in two successive time windows with a short sliding time is close, and the sliding time of $S_0 = 2$ s adopted in this paper is sufficiently small to a time window of $T_0 = 8$ s (generally $S_0 \geq T_0/2$) [30], the search range denoted by $[N_{\text{prev}} \quad \delta, \times\times\times, N_{\text{prev}} + \delta]$ is used to search HR for both $B_I(t)$ and $B_Q(t)$ data. Here $N_{\text{prev}}$ is the previous estimated HR, and search bound is $\delta = 10$ BPM. Through selecting the peak with the largest power in the given search range, on the spectra reconstructed respectively by $B_I(t)$ and $B_Q(t)$, the HR is estimated by the corresponding frequency that we name current estimation $N_{\text{cur}}$.

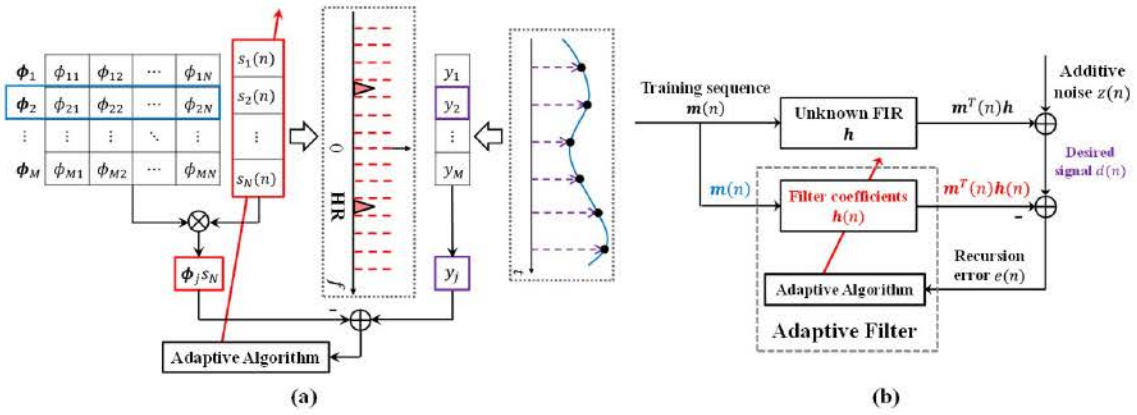


Figure 3-3: Adaptive filter framework to solve SSR problem. (a) SSR problem. (b) Unknown FIR and adaptive filter

3. Verification: Due to the noise components on the spectra, some probably wrong HR estimations cannot be avoided. To cope with an overmuch abrupt HRV that is abnormal in a short period, $N_{\text{cur}}$ is replaced by $N_{\text{prev}}$ if $\|N_{\text{prev}} \quad N_{\text{cur}}\|$ is bigger than some threshold, such as experimental 6 BPM.

## 3.2 ZA-SLMS Algorithm for SSR

In our proposed framework, SSR is regraded as a key part. Fig. 3-3(a) intuitively shows the objective of SSR problem, namely, to reconstruct the original heartbeat spectrum by an updating signal $\mathbf{s}(n)$, relying on the samples of radar signal $\mathbf{y}'$ and a given basis matrix $\mathbf{\Phi}$. Eventually, a reconstructed spectrum $\|s_k(n)\|^2$, $k \ / \}1, \times\times, N|$ can be obtain by the steady-state $\mathbf{s}(n)$, and it will be dealt with in the following tracking of spectral peak.

### 3.2.1 Adaptive Filter

Adaptive filter has drawn great attentions for a long time, due to its simple structure and reliable performance facing interference [56,57], which is the premise of the usage of adaptive-type algorithms, including our proposed ZA-SLMS and IZA-SLMS. A popular adaptive filter framework is shown in Fig. 3-3(b), which features in the

Table 3.1: Parameters correspondences between SSR problem and adaptive filter

| SSR Problem | Adaptive Filter |
|---|---|
| $\phi_j$ | $\mathbf{m}^{\mathrm{T}}(n)$ |
| $\mathbf{s}(n)$ | $\mathbf{h}(n)$ |
| $y_j$ | $d(n)$ |

estimation of unknown finite impulse response (FIR) $\mathbf{h} = [h_1, h_2, \ldots, h_N]^{\mathrm{T}}$ by the critical adaptive filter. More concretely, the recursion error

$$e(n) = d(n) \quad \mathbf{m}^{\mathrm{T}}(n)\mathbf{h}(n) \tag{3.6}$$

is extracted to construct the cost functions of adaptive algorithms, the filter coefficients $\mathbf{h}(n) = [h_1(n), h_2(n), \ldots, h_N(n)]^{\mathrm{T}}$ are iteratively reconstructed to estimate $\mathbf{h}$. Here $d(n) = \mathbf{m}^{\mathrm{T}}(n)\mathbf{h} + z(n)$ is the inner-product of input signal

$$\mathbf{m}(n) = [m(n), m(n \quad 1), \ldots, m(n \quad N+1)]^{\mathrm{T}} \tag{3.7}$$

termed training sequence and $\mathbf{h}$, contaminated by additive noise $z(n)$.

In view of the feasibility that sparse signal can be reconstructed by adaptive filter [34], in this paper, heartbeat spectrum is reconstructed based on the correspondences of parameters between SSR problem and adaptive filter shown in Table 3.1. As shown in Fig. 3-3, the row vectors $\phi_j$, $j$ / }1, ××, $M|$ in $\Phi$ acting as $\mathbf{m}(n)$ and the corresponding element in $\mathbf{y}'$ acting as $d(n)$, are used circularly, to make $\mathbf{s}(n)$ to reach steady-state.

### 3.2.2 ZA-SLMS Algorithm

Based on adaptive filter, the proposed ZA-SLMS algorithm is described here. Least-mean-square (LMS) algorithm is a popular adaptive algorithm due to its simplicity and practicability [56, 57], and many sparse versions have been developed [39, 44, 58]. Since the recursion updating equation of the ZA-SLMS algorithm is derived from the

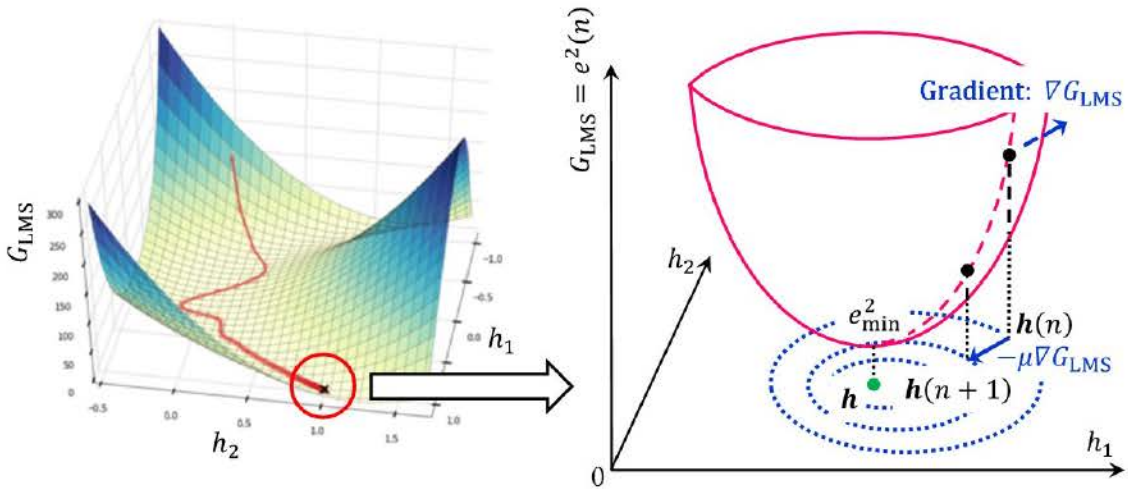


Figure 3-4: Gradient descent in the case of LMS algorithm.

zero-attracting least-mean-square (ZA-LMS) algorithm [58], the cost function of the ZA-LMS is recalled:

$$G_{\text{ZA-LMS}} = \underbrace{e^2(n)}_{\text{gradient correction}} + \underbrace{\lambda \|\mathbf{h}(n)\|_1}_{\text{sparse penalty}}, \tag{3.8}$$

where $\mu$ is a step-size decides the convergence rate, $\lambda$ is a REPA that trades off the gradient correction and the sparse penalty, and $\|\cdot\|_1$ is the Euclidean $\ell_1$-norm. The recursion updating equation is derived by the gradient $G_{\text{LMS}}$ as follows,

$$\mathbf{h}(n+1) = \mathbf{h}(n) + \underbrace{\mu e(n)\mathbf{m}(n)}_{\text{gradient correction}} \underbrace{\gamma \text{sgn}(\mathbf{h}(n))}_{\text{sparse penalty}}, \tag{3.9}$$

where $\gamma = \mu\lambda$ termed zero attraction factor plays a similar role with $\lambda$, i.e., to balance the proportion between the correction of gradient and sparse constraint, and the $\text{sgn}(\cdot)$ is a component-wise sign function defined as

$$\text{sgn}(x) = \begin{cases} \dfrac{x}{\|x\|}, & \text{if } x \neq 0, \\ 0, & \text{otherwise.} \end{cases} \tag{3.10}$$

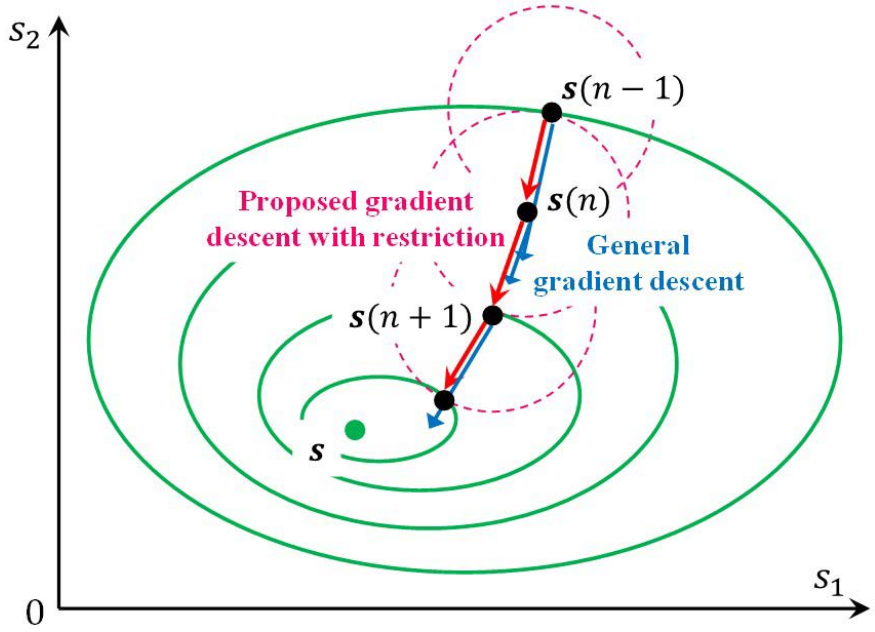


Figure 3-5: The comparison of general gradient descent and proposed gradient descent with restriction under impulsive noises

Fig. 3-4 intuitively shows the LMS algorithm-induced gradient descent, where $\mathbf{h}$ and $\mathbf{h}(n)$ are assumed to locate a plane denoted by $h_1$ and $h_2$, and $\mathbf{h}(n)$ approaches iteratively $\mathbf{h}$ by decreasing $G_{\text{LMS}}$ to the minimum $e^2_{\text{min}}$. In Eq. (3.8), the introduced sparse penalty benefits the exploitation of sparsity, resulting in the acquisition of more realistic heartbeat spectrum [39, 44, 58].

Furthermore, some literatures have clarified that many artificial or physical noises have impulsive nature departing from Gaussian distribution, including biological noise [59–61]. Such environments probably lead severe performance degradation to adaptive algorithms due to the unstable gradient descent, and the modification of gradient by restricting error $e(n)$ is regarded as an effective way to suppress sudden disturbance [39, 62]. Fig. 3-5 shows the updating process of restricted gradient descent, which enhances the stability of general gradient descent. Through quantifying the updating of $e(n)$, the recursion updating equation of ZA-SLMS algorithm is obtained,

$$\mathbf{h}(n+1) = \mathbf{h}(n) + \mu \text{sgn}(e(n))\mathbf{m}(n) \quad \gamma \text{sgn}(\mathbf{h}(n)). \tag{3.11}$$

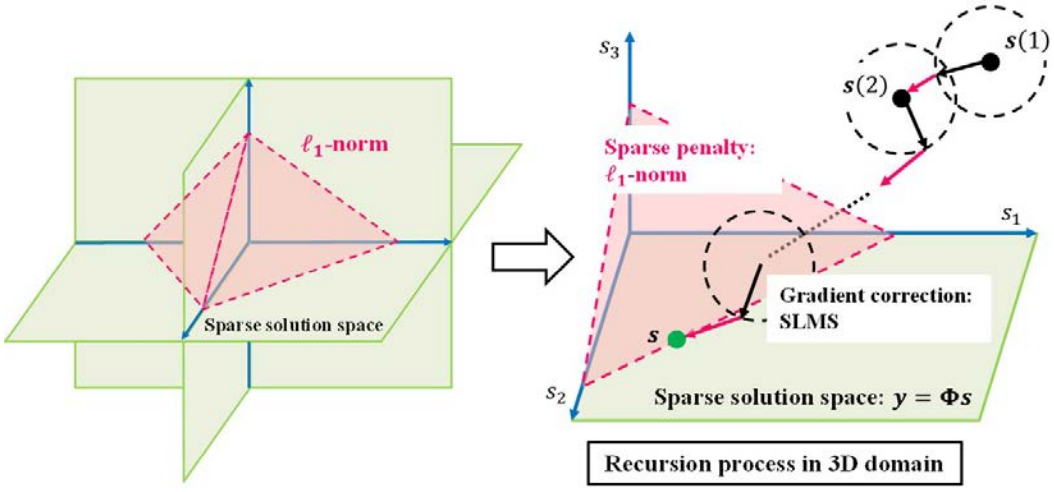


Figure 3-6: Recursion procedure of the ZA-SLMS algorithm

which consists of restricted gradient correction and $\ell_1$-norm-based sparse penalty. The recursion procedure of the ZA-SLMS algorithm is shown in Fig. 3-6. Through applying alternatively the gradient correction by LMS and the sparse constraint by $\ell_1$-norm on updating signal, the process of SSR by ZA-SLMS is summarized in Method 1.

## 3.3 Improved ZA-SLMS Algorithm

Although the ZA-SLMS algorithm can realize robustly SSR, it is difficult for this algorithm to always reach high-accurate HR estimation under various conditions, limited by the fixed weight of sparse constraint. The amplitude of radar signal varies significantly along with ambient environments, therein, the movements from subjects are regarded as one of the most causes [30, 31, 41]. Fig. 3-7 shows an intuitive comparison of amplitude variations of $B_I(t)$ and $B_Q(t)$ against different subjects' activities, one can find that the amplitude variations on typewriting accompanying body motion, are more obvious than those of sitting still. The obvious fluctuations of radar signal probably bring significant decrease of accuracy, due to an improper proportion between gradient correction and sparse penalty by a constant REPA $\lambda$. To better regulate the weight of sparse constraint dealing with different subjects'

**Method 1** ZA-SLMS algorithm for SSR

**Input:** $\mathbf{\Phi}$, $\mathbf{y}'$

**Output:** $\mathbf{s}(n)$

1: Initialize $\mathbf{s}(1) = \mathbf{0}$, $n = 1$, choose $\mu$, $\lambda$.

2: **while** $n < C$ ($C$ is a given maximum iteration run) **do**

$$\mathbf{m}^{\mathrm{T}}(n) = \phi_j,$$

$$d(n) = y_j,$$

where $j = \mathrm{mod}(n, M)$, with $\mathrm{mod}(\times)$ denotes the modulo function that calculate remainder of division.

3: Calculate recursion error

$$e(n) = d(n) \quad \mathbf{m}^{\mathrm{T}}(n)\mathbf{h}(n).$$

4: Correct gradient of $\mathbf{s}(n)$ by LMS

$$\mathbf{s}(n+1) = \mathbf{s}(n) + \mu \mathrm{sgn}(e(n))\mathbf{m}(n).$$

5: Penalize sparse constraint by $\ell_1$-norm

$$\mathbf{s}(n+1) = \mathbf{s}(n+1) \quad \gamma \mathrm{sgn}(\mathbf{s}(n)).$$

6: Iteration run increases by one

$$n = n + 1.$$

7: **end while**

activities, an adaptive REPA (REPA) is proposed to adaptively change the scale of REPA, by incorporating an improved ZA-SLMS algorithm named IZA-SLMS.

The proposed AREPA is given by

$$\lambda_{\mathrm{ada}} = \lambda \ \ \delta + \nabla_{\overline{\sigma}}[\ / \nabla_{\overline{\sigma}} \tag{3.12}$$

where $\lambda$ is an initial REPA, $\sigma$ is the standard deviation of $\mathbf{y}'$, and $\delta$ is the threshold of AREPA, respectively. The functions of $\sigma$ and $\delta$ are as follows:

- $\sigma$: To a small amplitude variation of $\mathbf{y}'$, $\lambda_{\mathrm{ada}}$ is set as a relatively large value by small $\sigma$, when the weight on sparse penalty correspondingly increases. In contrast, when the amplitude largely varies by strong MA, $\lambda_{\mathrm{ada}}$ relatively de-

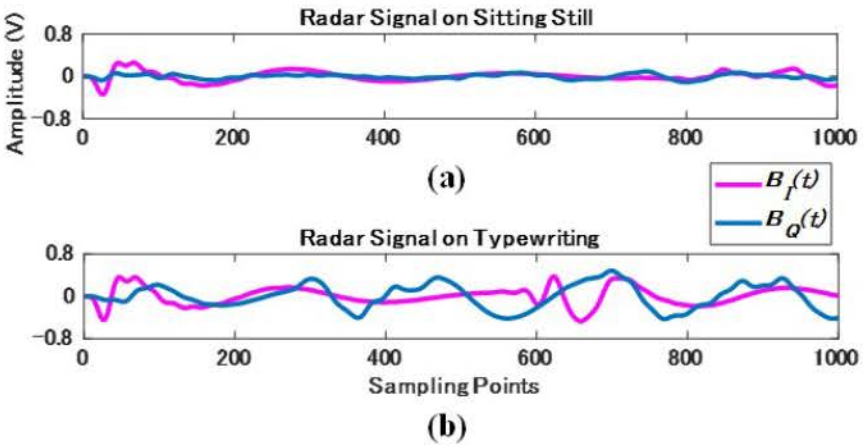


Figure 3-7: An example showing the comparison of the amplitudes of radar signal on different subjects' movements. (a) A segment of radar signal on sitting still. (b) A segment of radar signal on typewriting

creases due to a larger $\sigma$. Hence, a part of weight will be transferred to gradient correction from sparse penalty.

- $\delta$: To prevent an overmuch fast change of AREPA, $\delta$ is introduced to enhance the stability of proportion regulation, guaranteeing a reasonable acquisition of AREPA.

Based on the the cost function of the ZA-SLMS algorithm defined in Eq. (3.8), the cost function of further proposed IZA-SLMS algorithm is defined by introducing AREPA,

$$G = e^2(n) + \lambda_{\text{ada}} \sqrt{\mathbf{h}(n)} \sqrt{1}. \tag{3.13}$$

Similarly, the corresponding recursive updating equation is derived as

$$\mathbf{h}(n+1) = \mathbf{h}(n) + \mu \text{sgn}(e(n))\mathbf{m}(n) \quad \gamma_{\text{ada}} \text{sgn}(\mathbf{h}(n)), \tag{3.14}$$

where $\gamma_{\text{ada}} = \mu\lambda_{\text{ada}}$ is an adaptive zero attraction factor. In contrast to ZA-SLMS, an adaptive AREPA parameter is introduced into the cost function, and the process of SSR by the improved IZA-SLMS is summarized in Method 2.

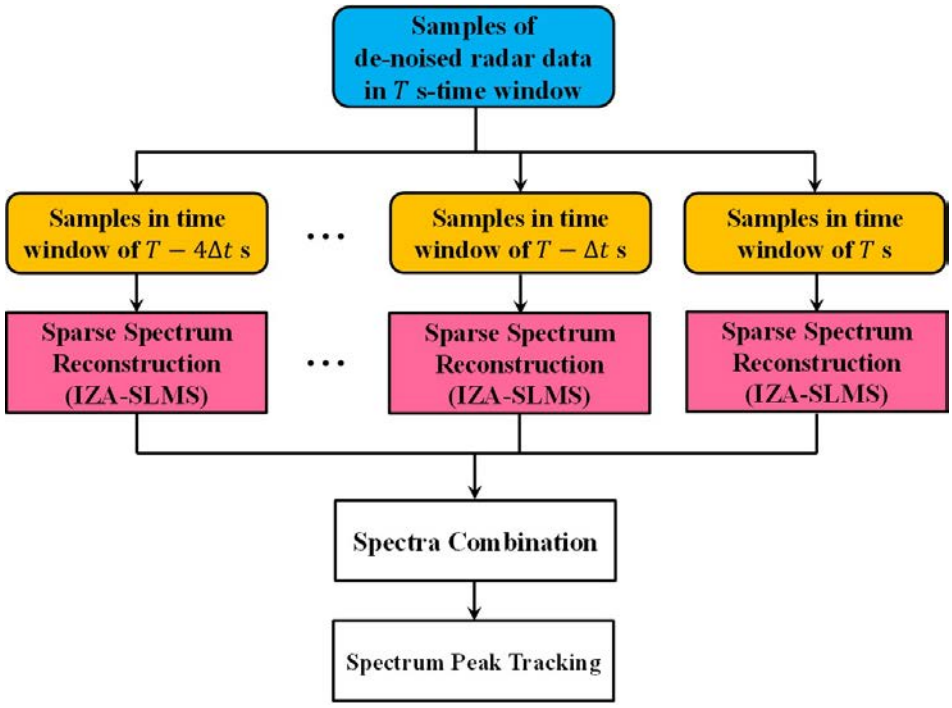


Figure 3-8: The flowchart of TWV framework incorporating IZA-SLMS algorithm for SSR

## 3.4 IZA-SLMS Algorithm Combining with TWV

Unlike the single time window used in most detection methods, TWV technique reconstructs the interested spectra by several time windows with slight length variation, namely length-varying samples of data. TWV makes it possible that higher accuracy is acquired, combining spectrum transform methods of FFT [14] or CWT [26]. In a time window with short-period, e.g., 5 s, the received radar signal contains only one or two respiration cycles, and just an approximate respiratory rate can be calculated by the limited cycles [14, 26]. Since a short time window cannot fully reveal the periodicity of a respiration signal, the approximate respiratory frequency typically varies depending on the choice of time windows with different size. In contrast, a heartbeat signal has more cycles than those of a respiration signal in a given time window, which are up to 3–6 times [14, 26]. Owing to the better reveal of the periodicity of a heartbeat signal, the HR can be more reliably acquired than respiratory rate in some way. In particular, when the length of time window varies, the location of spectral

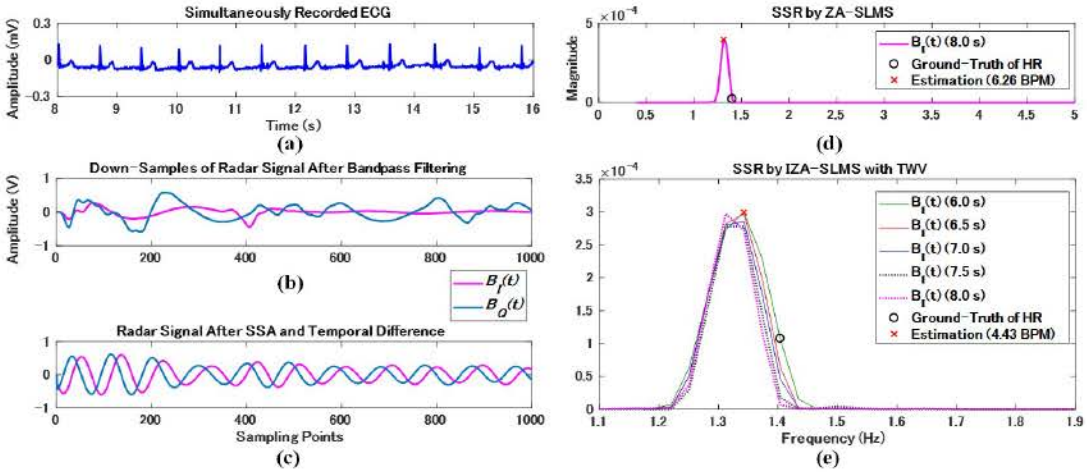


Figure 3-9: An example showing the benefit of TWV. (a) A segment of simultaneously recorded ECG signal regarded as the ground-truth of HR. (b) A segment of down-samples of radar signal after bandpass filtering. (c) The radar signal segment after SSA and temporal difference following (b). (d) SSR on (c) by ZA-SLMS. (e) SSR on (c) by IZA-SLMS with TWV

peak associated with HR is almost unchanged, which benefits the precise extraction of HR.

In view of the better adaptability against a variety of physical activities by the improved IZA-SLMS algorithm over the ZA-SLMS algorithm, the IZA-SLMS is adopted to realize SSR combining TWV technique. Fig. 3-8 elaborates the framework of TWV shown in Fig. 3-1, following the temporal difference, the samples of de-noised radar data in each time window of $T = 8$ s, are chosen as input data. To obtain a set of samples with varying lengths by input data, the time window changes by $T + i\Delta t$ s, $i \;/\; \}\quad 4,\quad 3, \times\times\times, 0|$ in order, which is close to the given length of $T$. By the fact that HR can be assumed to be unchanged under a short sliding time, i.e., $\Delta t < 0.1T$ [14], $\Delta t = 0.5$ s is experimentally set aiming to the 8 s-time window in this study. In comparison to the general SSR by single time window, in the case of TWV, the spectra reconstructed by the IZA-SLMS algorithm are combined for the final spectrum peak tracking.

An intuitive benefit of the incorporation of TWV is shown in Fig. 3-9. Through the relatively cleansed $B_I(t)$ and $B_Q(t)$ after the de-noising by bandpass filtering,

Table 3.2: Experimental parameters

| **Parameters** | **Specification** |
|---|---|
| Modulation type | Unmodulated CW |
| Carrier frequency | 24 GHz |
| Transmit power | 1 mW |
| Sampling frequency | 1 kHz |
| Height of radar | 80 cm |
| No. of subjects | Five |
| Observation duration | 2 minutes |
| Subjects' conditions | 1) Sitting still;<br>2) Typing with a laptop |
| Measuring distance $d_0$ | 1) 80 cm and supplemented 30 cm for sitting still;<br>2) 30 cm for typing |

SSA, and temporal difference, which exhibit heartbeat shown in Fig. 3-9(c), SSR is realized by the ZA-SLMS algorithm or the IZA-SLMS algorithm with TWV, as shown in Fig. 3-9(d) and Fig. 3-9(e). Fig. 3-9(e) shows a stable observation of spectral peaks corresponding to HR, namely the locations of peaks obtained by the time windows with five different lengths (6.0 s, 6.5 s, $\times\times\times$, 8.0 s) are almost unchanged, which brings about a smaller error of 4.43 BPM than that obtained by the ZA-SLMS (6.26 BPM). Note that the computational complexity of the IZA-SLMS algorithm with TWV directly depends on the number of adopted time windows, hence, its running time is approximately five times relative to that of the ZA-SLMS or the IZA-SLMS.

## 3.5 Experimental Results

In this chapter, experimental environment and results are presented, and analytical accuracy evaluation is performed to verify the advantage of our proposal. That is, the proposed SSR by the ZA-SLMS algorithms and its variants of IZA-SLMS and IZA-SLMS with TVW, and the proposed BSS by various NMF algorithms, namely standard NMF, SPNMF, and WSPNMF.

The parameters used in measurement are detailed in Table 3.2. The dataset

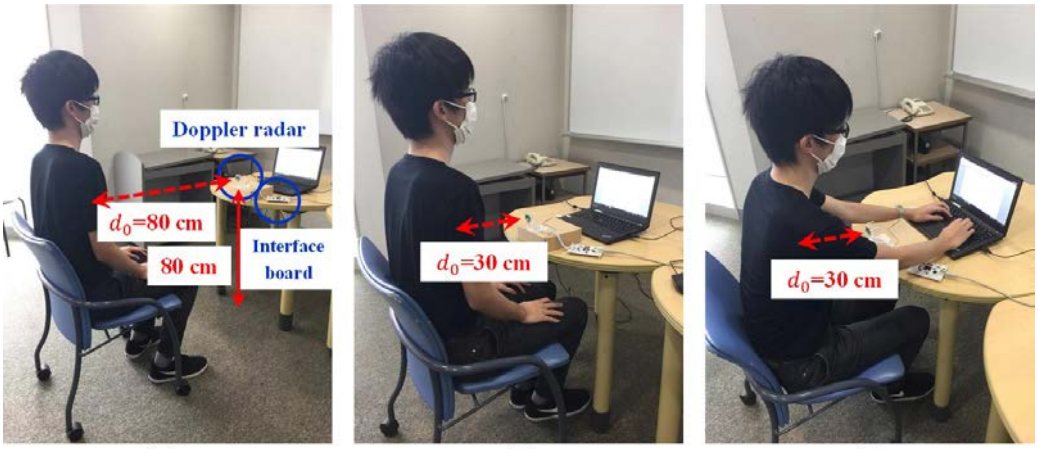


Figure 3-10: The setup of HR measurements against various subjects' activities. (a) Sitting still when basic $d_0 = 80$ cm. (b) Sitting still when supplemented $d_0 = 30$ cm. (c) Typing with a laptop when basic $d_0 = 30$ cm

consists of five 2-min recordings which were collected from 18 to 35 years old subjects performing various activities, i.e., sitting still or typing with a laptop. The ground-truth of HR is calculated by simultaneously recorded ECG signal, from the ECG sensor attaching a subject's chest. Setting at 80 cm-height, we used 24 GHz band Doppler radar with 1 kHz sampling frequency to detect heartbeat. The Doppler radar was positioned $d_0 = 80$ cm and 30 cm away from subjects, respectively against sitting still and typewriting as [40], and the basic radar setups are shown in Fig. 3-10(a) and 3-10(c). Note that the performance evaluation of HR estimation methods in the following subsection, is on the premise of basic measuring distance $d_0$. In addition, Fig. 3-10(b) shows the measurement at 30 cm-distance for sitting still, which is supplementarily conducted for further comparing performance with the case of typing at the same ranging.

To the Spectrogram method [16], the frequency band for integrate amplitudes is set 8–50 Hz, and the minimum and maximum peak-to-peak intervals are set 600 ms and 1000 ms, respectively. In order to exhibit the better robustness of the SGD-based SSR algorithms proposed in this paper, the proposed method using RM-FOCUSS algorithm [38] in SSR is applied for performance comparison. Referring to [30], the parameters of RM-FOCUSS, i.e., norm $p$ and REPA $\lambda_{\mathrm{RMF}}$ are set 0.8 and 0.1, respec-

tively.

The parameters of all the proposed sparse adaptive algorithms, i.e., the ZA-SLMS, the IZA-SLMS, and the IZA-SLMS with TWV, are chosen as follows:

- Step-size $\mu = 1 * 10^{-5}$, maximum iterations $C = 5 * 10^3$ for all the proposed algorithms,
- Zero attraction factor $\gamma_{\text{ZA}} = 2 * 10^{-6}$ for ZA-SLMS, $\gamma_{\text{IZA}} = 1 * 10^{-6}$ for the IZA-SLMS and IZA-SLMS with TWV, respectively,
- Threshold of AREPA $\delta = 0.8$ for IZA-SLMS and IZA-SLMS with TWV,
- Variation time of time windows $\Delta t = 0.5$ for IZA-SLMS with TWV.

One of the metrics for evaluating HR is average absolute error (AAE), which is calculated by the absolute value of the difference between the measured result and the ground-truth, as the following equation,

$$\text{AAE} = \frac{1}{N}\sum_{i=1}^{N} \|\text{BPM}_{\text{est}}(i) \quad \text{BPM}_{\text{true}}(i)\|, \tag{3.15}$$

where $\text{BPM}_{\text{est}}(i)$ and $\text{BPM}_{\text{true}}(i)$ respectively represent the estimated HR and ground-truth corresponding to the $i$-th time window. $N$ is the amount of time windows during an observation period. Since the metric of AAE has been widely used in HR estimation, as in [30, 41], we choose AAE as the primary metric for performance evaluation. The other metric of HR evaluation is AAE percentage (AAEP), which is defined as the ratio of AAE and ground-truth:

$$\text{AAEP} = \frac{1}{N}\sum_{i=1}^{N} \frac{\|\text{BPM}_{\text{est}}(i) \quad \text{BPM}_{\text{true}}(i)\|}{\text{BPM}_{\text{true}}(i)}. \tag{3.16}$$

Besides the two metrics of HR variation based on BPM, the root-mean-square error (RMSE) between the RRIs by estimation methods and reference signal, is also a common metric used in some literatures (see [16]). The average of RMSE is derived

Table 3.3: Average absolute error (AAE) of HR estimation [BPM]

(a) Sitting still

| | Subj 1 | Subj 2 | Subj 3 | Subj 4 | Subj 5 | Avg |
|---|---|---|---|---|---|---|
| **Spectrogram [16]** | 4.34 | 9.38 | 10.38 | 6.99 | 12.61 | 8.74 |
| **RM-FOCUSS [38]** | 5.14 | 3.79 | 3.72 | 3.22 | 5.07 | 4.18 |
| **ZA-SLMS** | 3.21 | 3.63 | 3.09 | 2.98 | 4.94 | 3.57 |
| **IZA-SLMS** | 2.42 | 3.87 | 2.65 | 3.37 | 4.72 | 3.40 |
| **IZA-SLMS with TWV** | 2.61 | 3.70 | 2.12 | 3.32 | 4.42 | 3.23 |

(b) Typing with a laptop

| | Subj 1 | Subj 2 | Subj 3 | Subj 4 | Subj 5 | Avg |
|---|---|---|---|---|---|---|
| **Spectrogram [16]** | 12.80 | 10.06 | 8.60 | 12.14 | 13.33 | 11.39 |
| **RM-FOCUSS [38]** | 3.12 | 5.08 | 2.93 | 7.18 | 4.45 | 4.55 |
| **ZA-SLMS** | 3.11 | 3.26 | 2.68 | 6.20 | 5.07 | 4.06 |
| **IZA-SLMS** | 3.23 | 3.14 | 2.74 | 5.83 | 5.08 | 4.00 |
| **IZA-SLMS with TWV** | 2.64 | 4.51 | 2.58 | 3.97 | 5.24 | 3.79 |

by

$$\mathrm{RMSE} = \sqrt{\frac{1}{N}\sum_{i=1}^{N} \|\mathrm{RRI}_{\mathrm{est}}(i) \quad \mathrm{RRI}_{\mathrm{true}}(i)\|^2}. \tag{3.17}$$

where $\mathrm{RRI}_{\mathrm{est}}(i)$ is the detected peak-to-peak interval of temporal signal, and $\mathrm{RRI}_{\mathrm{true}}(i)$ is the RRI acquired by ECG signal. The mentioned two estimations, i.e., $\mathrm{BPM}_{\mathrm{est}}(i)$ and $\mathrm{RRI}_{\mathrm{est}}(i)$, can be mutually transformed by the given expression,

$$\mathrm{RRI}_{\mathrm{true}}(i) = 60/\mathrm{BPM}_{\mathrm{est}}(i) * 10^3,\ i = 1,\ 2,\ \times\times\times,\ W, \tag{3.18}$$

which is helpful for the thorough performance assessment of our proposal.

The measurement accuracies of the three proposed algorithms are evaluated by two main indices, namely HR and RRI.

### 3.5.1 Performance Evaluation on HR

Table 3.3 and Table 3.4 present the AAE and AAEP on all 5 subjects' data recorded by Doppler radar, respectively. Using the three proposed algorithms (ZA-SLMS, IZA-

Table 3.4: Average absolute error percentage (AAEP) of HR estimation

(a) Sitting still

| | **Subj 1** | **Subj 2** | **Subj 3** | **Subj 4** | **Subj 5** | **Avg** |
|---|---|---|---|---|---|---|
| **Spectrogram [16]** | 5.8% | 12.1% | 14.5% | 9.9% | 14.5% | 11.4% |
| **RM-FOCUSS [38]** | 6.9% | 4.8% | 5.3% | 4.6% | 5.8% | 5.5% |
| **ZA-SLMS** | 4.3% | 4.6% | 4.4% | 4.2% | 5.6% | 4.6% |
| **IZA-SLMS** | 3.2% | 4.9% | 3.7% | 4.8% | 5.4% | 4.4% |
| **IZA-SLMS with TWV** | 3.5% | 4.7% | 3.0% | 4.7% | 5.0% | 4.2% |

(b) Typing with a laptop

| | **Subj 1** | **Subj 2** | **Subj 3** | **Subj 4** | **Subj 5** | **Avg** |
|---|---|---|---|---|---|---|
| **Spectrogram [16]** | 16.5% | 14.1% | 11.5% | 15.5% | 15.4% | 14.6% |
| **RM-FOCUSS [38]** | 4.0% | 7.2% | 3.8% | 9.5% | 5.1% | 5.9% |
| **ZA-SLMS** | 4.0% | 4.6% | 3.6% | 8.1% | 5.8% | 5.2% |
| **IZA-SLMS** | 4.1% | 4.4% | 3.6% | 7.6% | 5.8% | 5.1% |
| **IZA-SLMS with TWV** | 3.4% | 6.3% | 3.5% | 5.0% | 6.0% | 4.8% |

SLMS, and IZA-SLMS with TWV) can obtain more accurate HR estimation than the typical existing detection methods, under the status of sitting still or typing. More concretely, when subjects are sitting still, a smaller average AAE of 3.57 BPM is obtained by ZA-SLMS, compared with the Spectrogram method and the usage of RM-FOCUSS, as shown in Table 3.3(a). Moreover, the improved IZA-SLMS that can adaptively regulate the weight of sparse penalty further reduced the AAE to 3.40 BPM, and the smallest 3.23 BPM is achieved by IZA-SLMS with TWV. Although very few literatures can clarify the threshold for a qualified AAE, in general, a value less than 5.0 BPM is regarded as acceptable. Fortunately, the proposed algorithms typically can acquire acceptable AAEs that are less than 5.0 BPM.

In particular, in the case of typing with a laptop, Table 3.3(b) shows that a significant degradation of performance happened to the Spectrogram method, and certain degradation to RM-FOCUSS due to the vulnerability to strong noises. In contrast, the three proposed algorithms (ZA-SLMS, IZA-SLMS, and IZA-SLMS with TWV) achieve the reliable results of HR estimation around 4 BPM, due to the robustness to MA. Among our proposal, the IZA-SLMS with TWV still achieves the highest

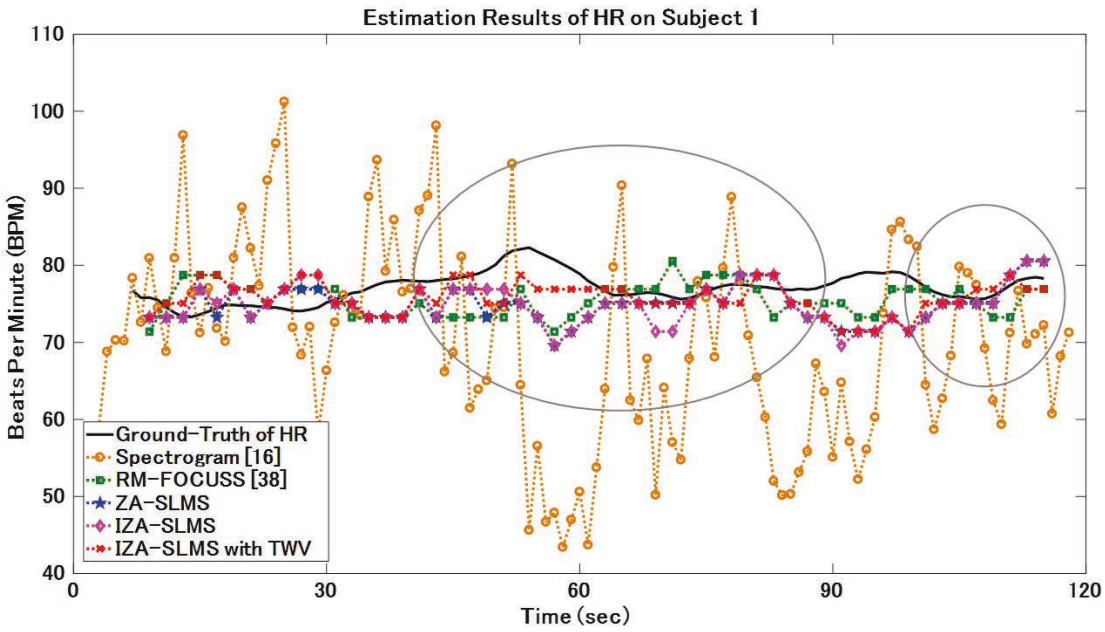


Figure 3-11: An example showing the comparison of the variation of HR estimated by detection methods, under typing with a laptop by Subject 1

accuracy owing to more stable HR detection by TWV.

Table 3.4 shows AAEP results of each method, which are basically consistent with the results of AAE in Table 3.3. Be superior to the Spectrogram method and RM-FOCUSS, our proposal obtains better HR estimation by smaller AAEP. Specifically, the IZA-SLMS with TWV respectively achieves the smallest AAEPs of 4.2% and 4.8%, against the two activities of sitting still and typing.

To intuitively show the performance superiorities of our proposal against the noises from respiration or body motion, the comparison of the HRV by different detection methods aiming to a subject in typing, is shown in Fig. 3-11. The interference caused by subjects' movements results in obvious deviation of HR estimation, to the ground-truth of HR by the Spectrogram method. While, the estimated HRs by the three proposed algorithms are generally more close to the variation of ground-truth. In particular, the IZA-SLMS with TWV most faithfully reflects HRV depending on the improved stability, and the observation periods when it evidently outperforms the other involved methods are highlighted by circles. Although our proposal does not tightly track the ground-truth of HR during some periods of time, due to interference

Table 3.5: Root-mean-square error (RMSE) of RRI estimation [ms]

(a) Sitting still

| | Subj 1 | Subj 2 | Subj 3 | Subj 4 | Subj 5 | Avg |
|---|---|---|---|---|---|---|
| **Spectrogram [16]** | 60 | 163 | 173 | 119 | 167 | 136 |
| **RM-FOCUSS [38]** | 66 | 49 | 51 | 55 | 53 | 55 |
| **ZA-SLMS** | 42 | 49 | 43 | 54 | 49 | 47 |
| **IZA-SLMS** | 32 | 52 | 35 | 54 | 48 | 44 |
| **IZA-SLMS with TWV** | 35 | 49 | 29 | 53 | 44 | 42 |

(b) Typing with a laptop

| | Subj 1 | Subj 2 | Subj 3 | Subj 4 | Subj 5 | Avg |
|---|---|---|---|---|---|---|
| **Spectrogram [16]** | 218 | 188 | 142 | 203 | 183 | 187 |
| **RM-FOCUSS [38]** | 39 | 62 | 41 | 82 | 45 | 54 |
| **ZA-SLMS** | 42 | 44 | 36 | 68 | 47 | 47 |
| **IZA-SLMS** | 43 | 42 | 36 | 63 | 50 | 47 |
| **IZA-SLMS with TWV** | 35 | 62 | 34 | 51 | 48 | 46 |

of respiration and movement, the instantaneous absolute error of estimation can be guaranteed in a small range. The similar phenomenon also happens to the proposed NMF algorithms in BSS approach, in Chapter 4.

### 3.5.2 Performance Evaluation on RRI

The RMSEs of the proposed three algorithms (ZA-SLMS, IZA-SLMS, and IZA-SLMS with TWV) can be obtained, which are summarized in Table 3.5. Similarly, our proposal (ZA-SLMS, IZA-SLMS, and IZA-SLMS with TWV) generally obtains smaller RMSEs over the Spectrogram method and RM-FOCUSS, toward to five subjects. Also, the three proposed algorithms exhibit the performance superiority, by the acquisition of smaller average RMSE to various subjects' activities. In particular, in the status of typing accompanying movements, the smallest RMSE of 46 ms can also be achieved by the IZA-SLMS with TWV, as shown in Table 3.5(b).

In fact, to different subjects, HR variability and strengths of respiration are typically distinct, which directly relates with the effect of HR estimation via Doppler radar. Hence, the further proposed IZA-SLMS and IZA-SLMS with TWV, can not

always obtain better HR estimation than the ZA-SLMS algorithm, against each subject. The similar phenomenon also happens to the proposed NMF algorithms in BSS approach, in Chapter 4.

**Method 2** IZA-SLMS algorithm for SSR

**Input:** $\mathbf{\Phi}$, $\mathbf{y}'$

**Output:** $\mathrm{s}(n)$

1: Initialize $\mathrm{s}(1) = \mathbf{0}$, $n = 1$, choose $\mu$, $\lambda$, $\delta$.

2: **while** $n < C$ ($C$ is a given maximum iteration run) **do**

$$\mathbf{m}^{\mathrm{T}}(n) = \phi_j,$$

$$d(n) = y_j,$$

where $j = \mathrm{mod}(n, M)$, with $\mathrm{mod}(\times)$ denotes the modulo function that calculate remainder of division.

3: Calculate recursion error

$$e(n) = d(n) \quad \mathbf{m}^{\mathrm{T}}(n)\mathbf{h}(n).$$

4: Correct gradient of $\mathrm{s}(n)$ by LMS

$$\mathbf{s}(n+1) = \mathbf{s}(n) + \mu \mathrm{sgn}(e(n))\mathbf{m}(n).$$

5: Calculate standard deviation $\sigma$ of $\mathbf{y}'$.

6: Acquire AREPA and adaptive zero attraction factor

$$\lambda_{\mathrm{ada}} = \lambda \ \ \delta + \nabla_{\overline{\sigma}}[\ / \nabla_{\overline{\sigma}},$$

$$\gamma_{\mathrm{ada}} = \mu\lambda_{\mathrm{ada}}.$$

7: Penalize sparse constraint by $\ell_1$-norm

$$\mathbf{s}(n+1) = \mathbf{s}(n+1) \quad \gamma_{\mathrm{ada}}\mathrm{sgn}(\mathbf{s}(n)).$$

8: Iteration run increases by one

$$n = n + 1.$$

9: **end while**

# Chapter 4

# Proposed BSS Approach

Inspired by the inapplicability of SSA in HR monitoring via Doppler radar, in this chapter, we propose a BSS approach to directly separate the individual sources mixed in $C(t)$ by the NMF structure, avoiding extra spectrum modification required by SSA.

First, an enhanced framework of HR measurement using the proposed BSS approach is redescribed, based on Chapter 3. Then, the basic BBS model, and our unsupervised BSS approach and two NMF algorithms with sparseness constraints, are respectively depicted. Finally, the experimental results by multiple metrics are provided.

## 4.1 Enhanced HR Measurement Framework

The flowchart of the applied framework used for HR measurement is shown in Fig. 4-1, where the proposed BSS and the emerging SSR are two key parts. To pursue a relatively high frequency domain resolution within an applicable period, a time window of $T_0 = 8$ s is adopted for input signal $C(t)$, with a $S_0 = 2$ s-forward sliding, as in [30, 41]. Each part of the measurement framework is briefly stated, in order.

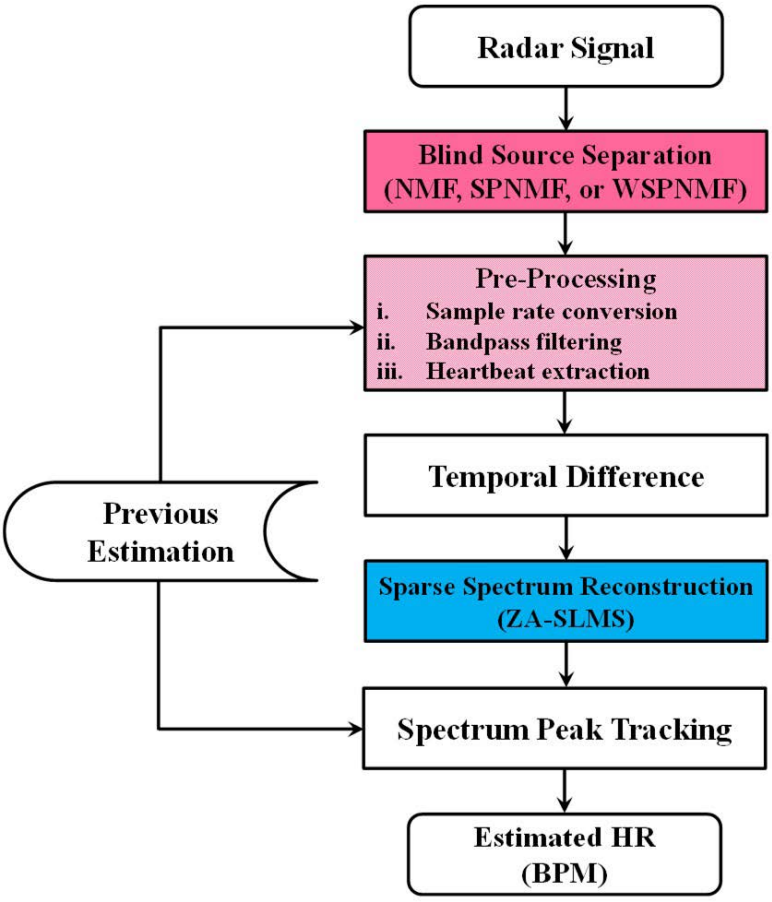


Figure 4-1: The flowchart of HR measurement framework, incorporating our proposed BSS approach

### 4.1.1 Blind Source Separation

In order to abstract the heartbeat source from the mixed radar signal, we propose an accuracte and practical BBS approach using NMF algorithms. In particular, not only standard NMF algorithm, two constrained NMF algorithms with sparseness, namely SPNMF [50] and WSPNMF, are also used to capture more partial representations of sources, by observing the time domain sparsity of targeted heartbeat. The details of the proposed BSS is elaborated in this chapter.

### 4.1.2 Pre-Processing

Followed by the BSS, the corresponding data pre-processing functions in pruning estimated signals and distinguishing the heartbeat, which consists of three steps: Step i. Sample rate conversion; Step ii. Bandpass filtering; Step iii. Heartbeat extraction. In the first step, to guarantee sufficient samples for SSR on the compromise of reasonable complexity, the $I$ composed components are converted to 125 Hz, referring to [30, 40]. Subsequently, the converted samples are bandpass filtered in the range of 0.4–5.0 Hz as [30, 40], covering a possible HR changes of 1.0–3.0 Hz [4]. At the last step, through searching the maximum peak occurring in the possible frequency band of HR, heartbeat component is extracted from $I$ "candidates", denoted as $\mathbf{z}$.

### 4.1.3 Following Parts

The following three parts, i.e., temporal difference, SSR, and spectrum peak tracking, inherit the ones of HR measurement framework shown in Fig. 3-1. Specifically, in the part of SSR, the ZA-SLMS algorithm is used without TWV, considering the trade-off between the performance and efficiency of estimation method.

## 4.2 Fundamental Model of BSS

For better illustrating our proposal, the fundamental BSS model is recalled as shown in Fig. 4-2, which is divided into the mixing process and the demixing process.

### 4.2.1 Linear Mixing Process

The mixture of $I$ sources can be simply assumed as linear [51], and the mixing model in discrete-time is given by

$$\mathbf{x}_f[t] = \Big[ \sum_{i}^{I} a_i \mathbf{s}_i[t] + \mathbf{v}[t],\ t\ /\ \}1, \times\times\times, T| \ , \tag{4.1}$$

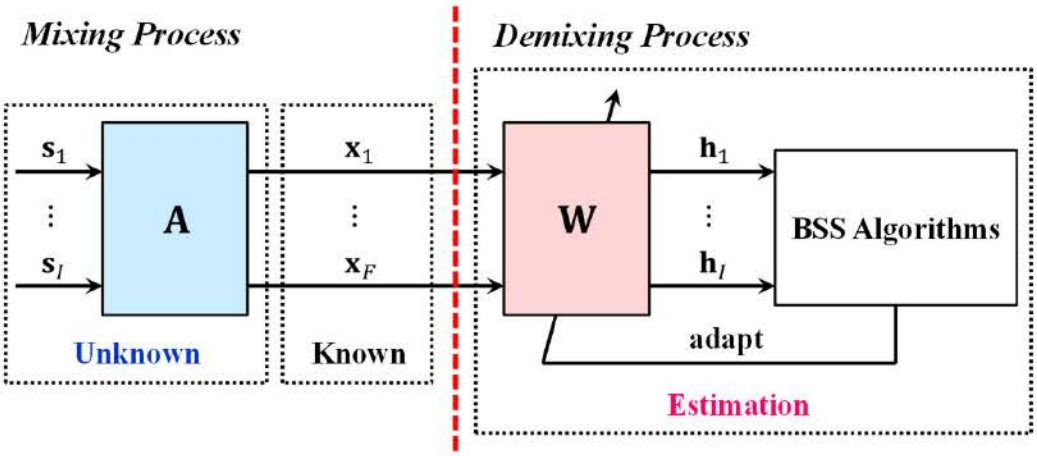


Figure 4-2: A fundamental BSS model consisting of the mixing process and the demixing process

where $\mathbf{s}_i[t]$ and $a_i$ denote a $T$-length of source signal and its amplitude, respectively. In consideration of additive noises $\mathbf{v}[t]$, such as white Gaussian, a mixture signal $\mathbf{x}_f[t]$, $f \;/\; \}1, \times\times\times, F|$ is observed as demixing objective. Neglecting the notion of discrete-time, the mixing process can be simply regarded as the multiplication of the unknown sources matrix $\mathbf{S} = ]\mathbf{s}_1^{\mathrm{T}}, \mathbf{s}_2^{\mathrm{T}}, \ldots, \mathbf{s}_I^{\mathrm{T}}\big(^{T} \;/\; \mathbb{R}^{I\times T}$ and the mixing matrix $\mathbf{A} \;/\; \mathbb{R}^{F\times I}$, with noise matrix $\mathbf{V} \;/\; \mathbb{R}^{F\times T}$. The corresponding matrix-form model of Eq. (4.1) can be obtained, i.e., $\mathbf{X} = \mathbf{AS} + \mathbf{V}$, where $\mathbf{X}$ is termed observation matrix. Note that the symbol $(\rangle_+$ that represents non-negative matrices is omitted in the following context, since the issue considered by the NMF algorithms used in this thesis, is within the non-negative variables.

### 4.2.2 Demixing Process by Standard NMF Algorithm

The intent of demixing is to separate individual sources $\mathbf{s}_i$ by estimating $\mathbf{h}_i$, through finding a separation matrix $\mathbf{W} \ll \mathbf{A}^{-1}$. By one or multiple known $\mathbf{x}_f$ in some form, the critical $\mathbf{W}$ is adaptively updated to obtain, adopting a proper BSS algorithm. In our method, practical NMF algorithms are used for BSS, which only requires single channel observation signal (sole $\mathbf{x}_f$), i.e., complex baseband signal $C(t)$.

Being good at multivariable and large amount of data, the algorithms of NMF

**Method 3** Standard NMF algorithm for BSS

**Input:** $\mathbf{X}$

**Output:** $\mathbf{W}$, $\mathbf{H}$

1: Initialize $\mathbf{W}$ and $\mathbf{H}$ by random uniform distribution subject to $(0, 1)$, choose number of basis vectors $K$ and upper bound of iterations $C_{\mathrm{NMF}}$. Set $n = k = f = t = 1$.

2: **while** $n \leqslant C_{\mathrm{NMF}}$ **do**

$$W_{fk}(n+1) = W_{fk}(n)\frac{]XH^{\mathrm{T}}(_{fk}}{[WHH^{\mathrm{T}}]_{fk}},$$

$$H_{kt}(n+1) = H_{kt}(n)\frac{]W^{\mathrm{T}}X(_{kt}}{[W^{\mathrm{T}}WH]_{kt}},$$

$$n = n + 1.$$

3: **end while**

along with extensions are broadly applied in signal/image processing, text mining, and data analysis, etc [45–48]. To specific applications, NMF can learn parts-based representations with various constraints, including indispensable non-negativity and optional sparseness, etc, enhancing the interpretability between objective and observation [45–48]. Recall the formula of NMF on matrix decomposition:

$$\mathbf{X} = \mathbf{WH} + \mathbf{E}, \tag{4.2}$$

where the observation matrix $\mathbf{X} \ / \ \mathbb{R}^{F\times T}$ is given by non-negative spectrogram of $C(t)$, which is factorized into two interactive factors, namely $\mathbf{W} \ / \ \mathbb{R}^{F\times K}$ and the estimation matrix $\mathbf{H} \ / \ \mathbb{R}^{K\times T}$, $K < \min\}F, T|$, considering unavoidable error represented by $\mathbf{E}$. The standard NMF algorithm only incorporates non-negativity constraint in Eq. (4.2), and a useful distance measure that is the square of Euclidean distance between $\mathbf{X}$ and $\mathbf{WH}$ constitutes the cost function:

$$D_{\mathrm{EUD}} = \sqrt{\mathbf{X} \quad \mathbf{WH}}^{2}_{F} = \Big[_{ft}\Big)X_{ft} \quad [WH]_{ft}\Big(^{2}, \tag{4.3}$$

where $\sqrt{\times}_F$ is Frobenius norm for matrices, and $t$ and $f$ represent time and frequency bin, respectively. The optimal condition is $\mathbf{X} = \mathbf{WH}$ that is equivalent to $\mathbf{E} = 0$,

when it reaches the lower limit of Eq. (4.3), i.e., zero. To minimize $D_{\mathrm{EUD}}$ subject to $W_{fk}, H_{kt} \approx 0$, the multiplicative update rules acting on $\mathbf{W}$ and $\mathbf{H}$ are derived based on the gradient descent:

$$W_{fk}(n+1) = W_{fk}(n)\frac{]XH^{\mathrm{T}}(_{fk}}{[WHH^{\mathrm{T}}]_{fk}}, \tag{4.4}$$

$$H_{kt}(n+1) = H_{kt}(n)\frac{]W^{\mathrm{T}}X(_{kt}}{[W^{\mathrm{T}}WH]_{kt}}, \tag{4.5}$$

where $n$ is the iteration number, and $k$ / $\}1, \times\times\times, K|$ . The multiplicative update skillfully avoids the sign changes to $\mathbf{W}$ and $\mathbf{H}$, and guarantees the non-increasing regression of Eq. (4.3). The standard NMF algorithm for BSS is summarized in Method 3.

## 4.3 BSS in Unsupervised Manner

The unsupervised manner proposed in our BSS approach achieves a practical HR observation by double clusterings, omitting additional training of heartbeat-only data that may require holding breath. The dynamic learning of BS within each time window adapts to the variation of HR over time, composed by three steps: the first clustering, the second clustering, and the learning of complete BS.

### 4.3.1 First Clustering

Based on NMF structure, the decomposition of whole mixture spectrogram $\mathbf{X}$ in the initial clustering is shown in Fig. 4-3(a), where $K = 20$ ($K > I$, as [51]) basis vectors $\mathbf{w}_k^{\mathrm{TW}}$ and the equal number of estimation signals $\mathbf{h}_k^{\mathrm{TW}}$ are obtained, respectively. Here, $\mathbf{w}_k^{\mathrm{TW}}$ are regarded as potential BS, used for optimizing the clustering at the second time. To capture periodicity of all sources, we can simply deal with the received radar signal in each time window with fixed length ($T_0 = 8$ s), which contains multiple cycles of the mixed source with the lowest frequency, i.e., respiration component [14, 26].

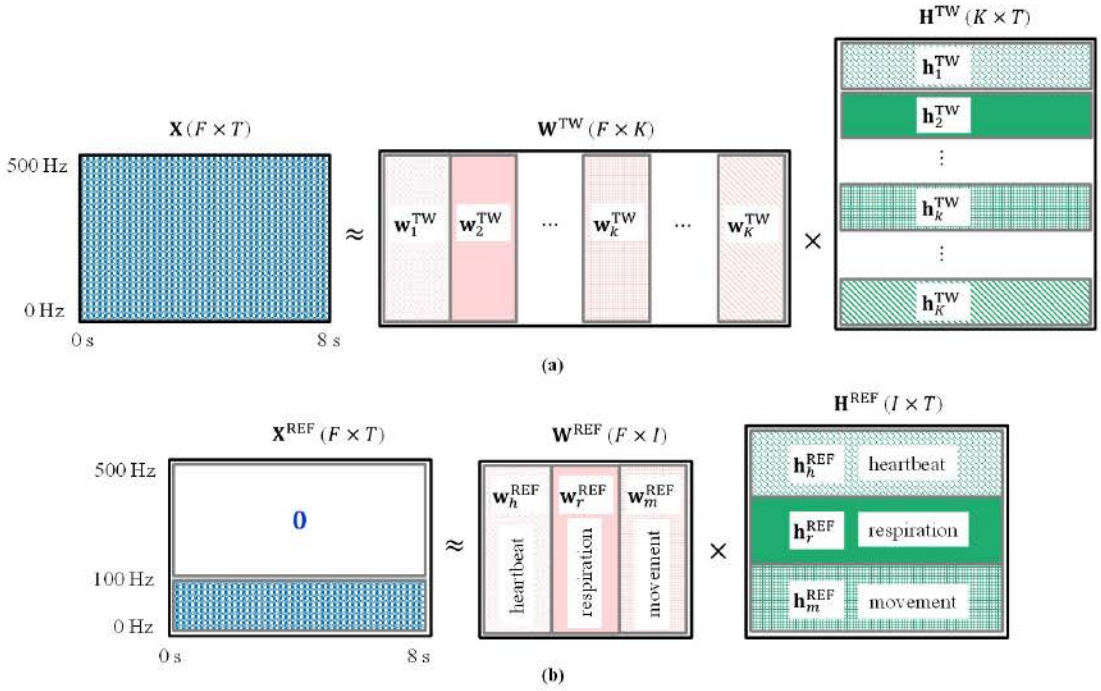


Figure 4-3: NMF-based decomposition of spectrogram of mixture signal. (a) First clustering for underlying BS. (b) Second clustering for RBS

Also, sufficient time-frequency bins are guaranteed by the choices of relatively large time window of 1.1 s and small forward sliding of 10 ms, in the usage of STFT for the generation of $\mathbf{X}$. Since Doppler radar operates at 1 kHz in our experiments, the maximum frequency of $\mathbf{X}$ is 500 Hz, where the spectral structure of $I$ sources is completely presented. Through factorizing $\mathbf{X}$ generated within one time window by the NMF algorithm, the underlying BS $\mathbf{W}^{\mathrm{TW}} = \left[\mathbf{w}_1^{\mathrm{TW}}, \cdots, \mathbf{w}_K^{\mathrm{TW}}\right]$ and the estimation matrix $\mathbf{H}^{\mathrm{TW}} = \left[\mathbf{h}_1^{\mathrm{TW}}{}^{\mathrm{T}}, \cdots, \mathbf{h}_K^{\mathrm{TW}}{}^{\mathrm{T}}\right]^{\mathrm{T}}$ are respectively acquired. We reserve $\mathbf{W}^{\mathrm{TW}}$ for the eventual BS learning, and discard $\mathbf{H}^{\mathrm{TW}}$.

### 4.3.2 Second Clustering

The intent of second clustering is to search the RBS of actual sources, which enables the activation of $\mathbf{W}^{\mathrm{TW}}$ from the first clustering. By the usage of prior knowledge, namely the number ($I = 3$) and the components of sources (heartbeat, respiration, and movement), we correspondingly modify $\mathbf{X}$ and the number of basis vectors as

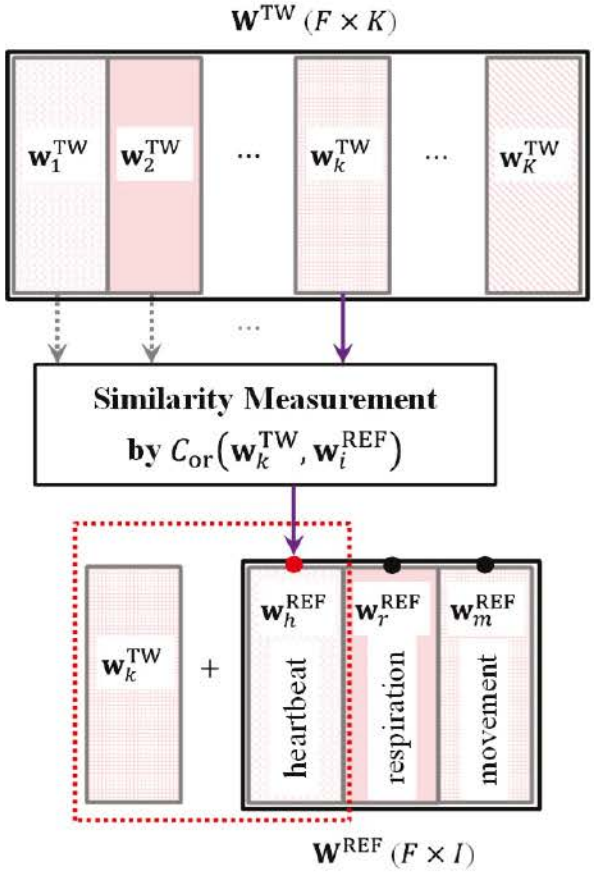


Figure 4-4: Learning of complete BS based on the similarity between underlying BS and RBS

reference. More concretely, only the frequency region that covers distinct magnitudes of heartbeat and respiration in $\mathbf{X}$, i.e., 0–100 Hz referring to [16], is retained, while the values of 100–500 Hz are replaced by zero, as intuitively shown in Fig. 4-3(b). By the NMF algorithm, the modified $\mathbf{X}$ denoted as $\mathbf{X}^{\mathrm{REF}}$ is decomposed into $I$ specific basis vectors $\mathbf{w}_i^{\mathrm{REF}}$, $i \ / \ \}h, r, m|$ , in an unfixed order, where $h$, $r$, and $m$ respectively represent cardiac, respiratory, and movement signal domains. We reserve the RBS $\mathbf{W}^{\mathrm{REF}} = \rceil \mathbf{w}_h^{\mathrm{REF}}, \mathbf{w}_r^{\mathrm{REF}}, \mathbf{w}_m^{\mathrm{REF}} \big($, as the foundation for learning complete BS, and discard $\mathbf{H}^{\mathrm{REF}} = \rfloor \ \mathbf{h}_h^{\mathrm{REF}} \lceil^{\mathrm{T}}, \ \mathbf{h}_r^{\mathrm{REF}} \lceil^{\mathrm{T}}, \ \mathbf{h}_m^{\mathrm{REF}} \lceil^{\mathrm{T}} \sqrt{}^{\mathrm{T}}$.

### 4.3.3 Complete BS Learning

Through similarity measurements on the resultant $\mathbf{W}^{\mathrm{TW}}$ and $\mathbf{W}^{\mathrm{REF}}$, the eventual BS learning is completed by hierarchical additions. In our method, a general correlation formula defined in [51] is given to measure similarity:

$$C_{\mathrm{or}}(\mathbf{f}_k, \mathbf{g}_k) = \frac{\sum \mathbf{f}_k \mathbf{g}_k}{\sqrt{\sum \mathbf{f}_k^2} \sqrt{\sum \mathbf{g}_k^2}}, \tag{4.6}$$

where $\mathbf{f}_k$ and $\mathbf{g}_k$ are two vectors with equal length. Obeying $[0, 1]$, $C_{\mathrm{or}}(\mathbf{f}_k, \mathbf{g}_k) = 0$ indicates the total uncorrelation between $\mathbf{f}_k$ and $\mathbf{g}_k$, in contrast, $C_{\mathrm{or}}(\mathbf{f}_k, \mathbf{g}_k) = 1$ represents that they are completely correlated when $\mathbf{f}_k$ and $\mathbf{g}_k$ are same.

Fig. 4-4 shows the learning procedure of complete BS. From the first basis vector in $\mathbf{W}^{\mathrm{TW}}$, i.e., $\mathbf{w}_1^{\mathrm{TW}}$, the "spectral correlation" between $\mathbf{w}_k^{\mathrm{TW}}$ and $\mathbf{w}_i^{\mathrm{REF}}$ is calculated one by one. Through similarity measurement, the spectral correlation is calculated by substituting $\mathbf{w}_k^{\mathrm{TW}}$ and $\mathbf{w}_i^{\mathrm{REF}}$ into Eq. (4.6),

$$C_{\mathrm{or}}(\mathbf{w}_k^{\mathrm{TW}}, \mathbf{w}_i^{\mathrm{REF}}). \tag{4.7}$$

The $\mathbf{w}_i^{\mathrm{REF}}$ with the maximum spectral correlation to current $\mathbf{w}_k^{\mathrm{TW}}$ is chosen as the componential target ($\mathbf{w}_h^{\mathrm{REF}}$, $\mathbf{w}_r^{\mathrm{REF}}$, or $\mathbf{w}_m^{\mathrm{REF}}$), which is added by the current $\mathbf{w}_k^{\mathrm{TW}}$. After the additions by all $\mathbf{w}_k^{\mathrm{TW}}$, $k \ / \ \}1, \times\times\times, K|$ , $\mathbf{W}^{\mathrm{REF}}$ is updated to complete BS $\hat{\mathbf{W}} = [\hat{\mathbf{w}}_h, \hat{\mathbf{w}}_r, \hat{\mathbf{w}}_m]$. Using $\hat{\mathbf{W}}$, $\mathbf{X}$ can be directly factorized to obtain the objective estimation matrix $\hat{\mathbf{H}} = \left]\hat{\mathbf{h}}_h, \hat{\mathbf{h}}_r, \hat{\mathbf{h}}_m \sqrt{\right.}$ and the heartbeat component $\hat{\mathbf{h}}_h$ will be extracted in the following pre-processing part.

## 4.4 Constrained NMF Algorithms with Sparseness

Although the standard NMF algorithm could accomplish the proposed BSS approach, sole non-negative penalization does not comprehensively reflect the characteristics of matrix factors, i.e., $\hat{\mathbf{W}}$ and/or $\hat{\mathbf{H}}$. This issue implies the necessity to extend the cost function in Eq. (4.3), by introducing additional auxiliary constraints [47, 48].

Correspondingly, the extended cost function with penalty terms is given by

$$D_{\text{CON}} = \sqrt{\mathbf{X} \quad \mathbf{WH}}_F^2 + \alpha J_1(\mathbf{W}) + \beta J_2(\mathbf{H}), \tag{4.8}$$

where vector-wise $J_1(\mathbf{W})$ and $J_2(\mathbf{H})$ enforce constraints depending on certain applications, and $\alpha$ and $\beta$ are constant regularization parameters that trade-off approximation error $\mathbf{E}$ and constraints.

### 4.4.1 Sparseness Constraint to NMF

In this study, we concentrate on the temporal sparsity of heartbeat source that exists in $\mathbf{H}$, and Eq. (4.8) can be simplified as

$$D_{\text{SPA}} = \sqrt{\mathbf{X} \quad \mathbf{WH}}_F^2 + \beta J_2(\mathbf{H}), \tag{4.9}$$

where $J_2(\mathbf{H})$ is the constraint of sparseness. [1] Based on the relationship between $\ell_1$-norm $\sum|y_i\|$ and $\ell_2$-norm $\sqrt{\sum y_i^2}$, a famous metric of sparseness degree [51] is defined as follows,

$$\text{sparseness}(\mathbf{y}) = \frac{\nabla_{\overline{N}} \quad (\sum|y_i\|) / \sqrt{\sum y_i^2}}{\sqrt{N} \quad 1}, \; i \; / \; \}1, \times\times, N| \; , \tag{4.10}$$

where $N$ is the dimensionality of considered signal $\mathbf{y}$, and sparseness($\mathbf{y}$) subjects to $[0, 1]$. Here, a low level of sparseness is represented by small sparseness($\mathbf{y}$), when $\mathbf{y}$ has most active elements, resulting in a large ratio between $\ell_1$-norm and $\ell_2$-norm. Whereas, large sparseness($\mathbf{y}$) represents a high level of sparseness, when most elements of sparseness($\mathbf{y}$) are zero or close to zero, resulting in a small ratio between $\ell_1$-norm and $\ell_2$-norm. Through enforcing proper degree of sparseness on $\mathbf{H}$, a more realistic heartbeat estimation $\hat{\mathbf{h}}_h$ in $\hat{\mathbf{H}}$ can be reconstructed, by the proposed SPNMF algorithm [50] or the improved WSPNMF algorithm.

[1] Prof. Ikehara: The explanation of Eq. (4.10) is not very sufficient.

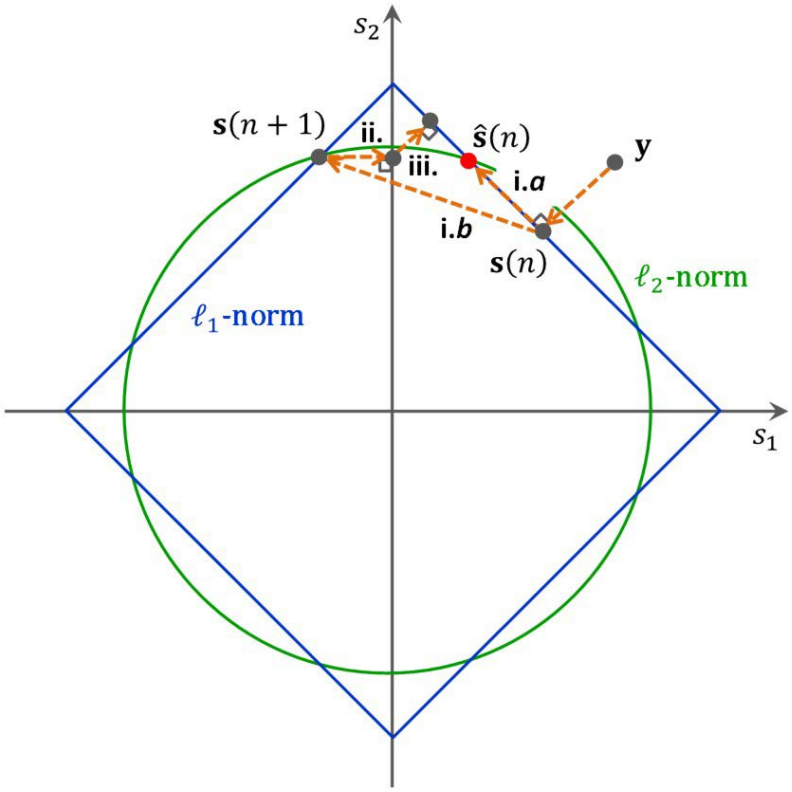


Figure 4-5: Intuitive illustration of projection function with joint constraint of $\ell_1$-norm and $\ell_2$-norm

### 4.4.2 Sparse NMF Algorithm

Unlike the standard NMF algorithm that only takes action in the descent of gradient with inverse direction, for minimizing the error $\mathbf{E}$ between $\mathbf{X}$ and $\mathbf{WH}$, the SPNMF algorithm further introduces the projection on joint constraint space [50], which is applied in the proposed double clusterings. In the SPNMF algorithm, the assumed sparseness of $\mathbf{H}$ represented by $S_{\mathbf{H}}$ needs pre-set, and the projection function $P(\mathbf{y}, L_1, L_2)$ plays the most important role in two aspects, where $L_1$ and $L_2$ are respectively the scales of $\ell_1$-norm and $\ell_2$-norm. Note that a large $S_{\mathbf{H}}$ brings about a small $L_1$, which facilitates the estimated sources $\hat{\mathbf{H}}$ to be sparse, vice versa. Also, when $S_{\mathbf{H}}$ is an empty set $\varnothing$, the SPNMF algorithm just reduces to the standard NMF algorithm. One effect of projection function is strictly setting $L_1$ that sparsifies the input $\mathbf{y}$, and $L_2$ that stabilizes updating of $\mathbf{y}$. The other effect is making the output

**Method 4** SPNMF algorithm for BSS

**Input:** **X**

**Output:** **W**, **H**

1: Initialize non-negative **W** and **H** by random Gaussian distribution, choose number of basis vectors $K$ and upper bound of iterations $C_{\text{SPNMF}}$. Set $S_{\mathbf{H}}$ / $[0,1]$ and $n = k = f = t = 1$.

$$L_1 = \nabla_{\overline{T}} \quad )^{\nabla_{\overline{T}}} \quad 1\Big( S_{\mathbf{H}},$$

where $T$ is the number of columns of **H**. Initially invoke the projection function,

$$\mathbf{h}_k(n) = P\left(\mathbf{h}_k(n), L_1, 1\right), \; k \; / \; \}1, \times\times\times, K| \; .$$

2: **while** $n \leqslant C_{\text{SPNMF}}$ **do**

$$W_{fk}(n+1) = W_{fk}(n)\frac{]XH^{\mathrm{T}}\big(_{fk}}{[WHH^{\mathrm{T}}]_{fk}}.$$

3: Implement additive gradient descent to **H** as follows,

$$H_{kt}(n+1) = H_{kt}(n) \quad \mu]W^{\mathrm{T}}(WH \quad X)\big(_{kt},$$

4: Invoke the projection function,

$$\mathbf{h}_k(n+1) = P\left(\mathbf{h}_k(n+1), L_1, 1\right),$$

$$n = n + 1.$$

5: **end while**

of $P(\mathbf{y}, L_1, L_2)$ non-negative, which coincides with the essential principle of the NMF algorithms.

Fig. 4-5 intuitively illustrates the joint constraint-induced projection function. After initially projecting $\mathbf{y}$ onto the hypersphere of $\ell_1$-norm obeying $L_1 = \sum \|s_i(n)\|$, when $n = 1$, the following iteration procedure of projection function can be divided into three steps: Step i. Within the constraint space where $L_1 = \sum \|s_i(n)\|$ and $L_2 = \sum s_i^2(n)$, $\mathrm{s}(n)$ is projected to the intersection of $\ell_1$-norm and $\ell_2$-norm with the closest distance to obtain $\mathrm{s}(n+1)$, when error may occur. For the *Case a*, if all the coefficients of $\mathrm{s}(n+1)$ are non-negative, i.e., $s_i(n+1) \geqslant 0, \cup i$, the current $\mathrm{s}(n+1)$ is output as the final result $\hat{\mathrm{s}}(n)$. For the *Case b*, if some coefficients of $\mathrm{s}(n+1)$ are subtractive, the subtractive values are replaced by zeros, as Step ii.. Finally,

at Step iii., the resultant $\mathbf{s}(n+1)$ is further fixed relying on $L_1$, and $\mathbf{s}(n+1)$ is sequentially updated from Step i. at the next iteration. The SPNMF algorithm for BSS is summarized in Method 4, and the invoked projection function is depicted in Method 4.

### 4.4.3 Weighted Sparse NMF Algorithm

Furthermore, through observing the evident difference of sparseness between heartbeat and the other ($I$ 1) sources, the WSPNMF algorithm penalizes weighted sparseness constraints to each updating estimation signal $\mathbf{h}_i^{\mathrm{REF}}$, $i$ / $\}h, r, m|$ in the second clustering, over the uniform constraint of the SPNMF algorithm. Besides dominant sparsity, heartbeat signal also has more prominent periodicity than respiration and movements, which corresponds to larger proportion of sparseness constraint. More concretely, when $\mathbf{h}_i^{\mathrm{REF}}$ have been preliminarily reconstructed by $\mathbf{h}_k(n+1)$, $k$ / $\}1, \times\times\times, I|$ after half of maximum iterations $C_{\mathrm{WSPNMF}}$, we measure their standard deviations of first-order temporal difference that reflects periodicities. Correspondingly, a set of regularization parameters $\Lambda = [\lambda_1, \times\times\times, \lambda_k, \times\times\times, \lambda_I]$ are given to respectively regulate $L_1$ that is the scale of sparseness constraint, namely, moderately small $\lambda_k$ for large standard deviation, vice versa. Here, $\lambda_k$ is formulized as

$$\lambda_k = \delta + \eta R_k, \tag{4.11}$$

with $R_k = 1/\mathrm{std}\left(\mathrm{diff}\left(\mathbf{h}_k(n+1)\right)\right)$, where std(⨯ denotes a standard deviation function, and $\eta$ and $\delta$ are weight factor and threshold of $\lambda_k$, respectively. The WSPNMF algorithm for BSS is summarized in Method 6.

## 4.5 Experimental Results

In the experiments for evaluating the proposed BSS approach, the dataset, setting, and three metrics are same with those for the proposed SSR approach in Chapter 3. Note that, compared with the standard NMF algorithm, the further proposed

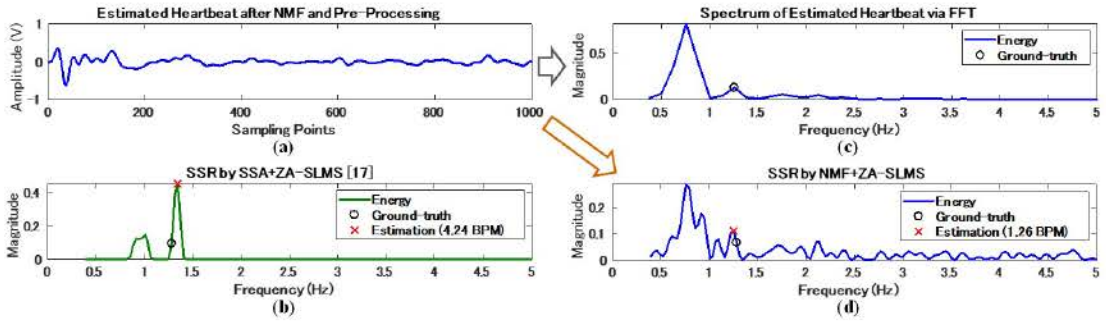


Figure 4-6: An example showing the benefit of NMF-based BSS under subjects' typing. (a) A segment of estimated heartbeat component extracted from Doppler signal after standard NMF and pre-processing. (b) SSR by ZA-SLMS after SSA. (c) Spectrum of estimated heartbeat component via FFT using (a). (d) SSR by ZA-SLMS after standard NMF using (a). All frequency domain signals in (b), (c), and (d) are normalized

constrained NMF algorithms with sparseness (SPNMF and WSPNMF) are able to improve the performances of HR estimation, by penalizing additional sparse constraints on updating estimation matrix $\mathbf{H}$ including heartbeat source. In addition, through implementing weighted sparse constraints, the WSPNMF algorithm can generally bring about more precise HR estimation, over that by the SPNMF algorithm with uniform sparse constraint.

As [40], the ZA-SLMS algorithm [39] was used for achieving SSR in this study, where the step-size is $1 * 10^{-5}$, maximum iterations is $5 * 10^{3}$, and the zero attraction factor $\gamma$ is respectively $2 * 10^{-6}$ and $2 * 10^{-11}$ when it combines with SSA and NMF algorithms. The parameters of the proposed NMF algorithms, i.e., standard NMF, and sparseness-constrained SPNMF and WSPNMF, were itemized:

- Upper bound of iterations $C_{\mathrm{NMF}} = 130$ for standard NMF as [51], $C_{\mathrm{SPNMF}} = 10$ for SPNMF referring to [50], and $C_{\mathrm{WSPNMF}} = 10$ for WSPNMF,
- Sparseness of $\mathbf{H}$ is set as $S_{\mathbf{H}} = 0.2$, both for SPNMF and WSPNMF,
- To WSPNMF, the weight factor is set as $\eta = 1 * 10^{-4}$, threshold of regularization parameters $\delta$ is respectively 0.990 and 0.994, to subjects' sitting still and typewriting conditions.

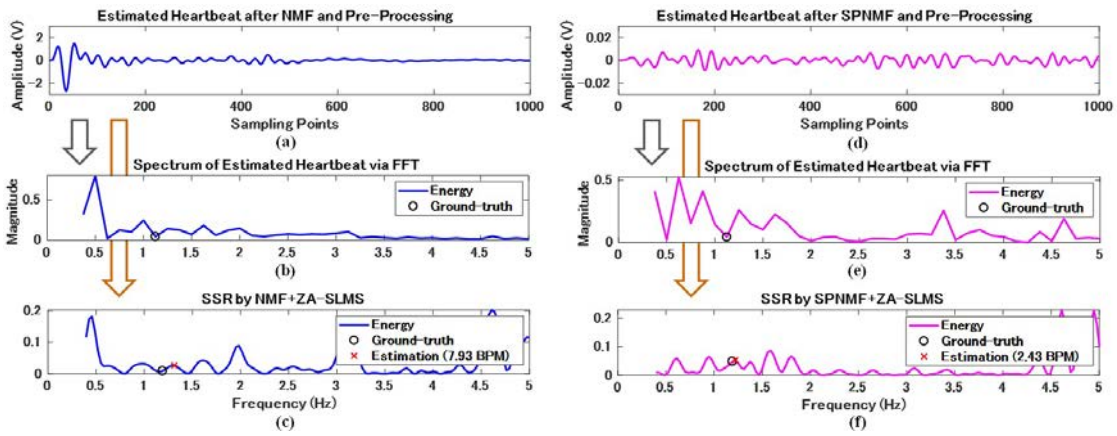


Figure 4-7: An example showing the benefit of sparseness constraint introduced in SPNMF under subjects' typing. (a) A segment of estimated heartbeat component extracted from Doppler signal after standard NMF and pre-processing. (b) Spectrum of estimated heartbeat component via FFT using (a). (c) SSR by ZA-SLMS after standard NMF using (a). (d) A segment of estimated heartbeat component extracted from Doppler signal after SPNMF and pre-processing. (e) Spectrum of estimated heartbeat component via FFT using (d). (f) SSR by ZA-SLMS after SPNMF using (d). All frequency domain signals in (b), (c), (e), and (f) are normalized

Figs. 4-6 and 4-7 intuitively show the benefits of the proposed BSS, respectively by standard NMF algorithm and SPNMF algorithm. In Fig. 4-6, when a subject types with a laptop, the noises from respiration and movements overlap the spectral location of realistic HR, resulting in performance degradation with error of 4.24 BPM, as shown in Fig. 4-6(b). Instead, owing to the demixing of mixture signal by standard NMF, the realistic HR-associated peak stands out within the normal frequency band of approximate 1.0–1.6 Hz (60–100 BPM) [20], which can be easily detected reducing the error to only 1.26 BPM. Moreover, the effect of introduced sparseness constraint in SPNMF is validated in Fig. 4-7, under the status of typewriting. Because the distinct characteristics of heartbeat including its sparsity and periodicity are neglected, at some times, the correct peak corresponding to HR nearly disappears in the probable frequency range, resulting in a large error of 7.93 BPM shown in Fig. 4-7(c). Instead, Fig. 4-7(f) shows that the penalization of sparseness helps the exploitation of cyclicity of heartbeat, guaranteeing reliable HR estimation with small error of 2.43 BPM.

Table 4.1: Average absolute error (AAE) of HR estimation [BPM]

(a) Sitting still

| | Subj 1 | Subj 2 | Subj 3 | Subj 4 | Subj 5 | Avg |
|---|---|---|---|---|---|---|
| **Spectrogram [16]** | 4.34 | 9.38 | 10.38 | 6.99 | 12.61 | 8.74 |
| **SSA+ZA-SLMS [40]** | 3.21 | 3.63 | 3.09 | 2.98 | 4.94 | 3.57 |
| **NMF+ZA-SLMS** | 2.29 | 3.72 | 2.82 | 3.36 | 4.78 | 3.39 |
| **SPNMF+ZA-SLMS** | 2.48 | 3.48 | 2.91 | 3.30 | 3.75 | 3.18 |
| **WSPNMF+ZA-SLMS** | 2.60 | 3.36 | 3.10 | 2.75 | 4.12 | 3.19 |
| **⩽NMF+ZA-SLMS** | 2.41 | 3.69 | 2.51 | 3.76 | 4.33 | 3.34 |
| **⩽SPNMF+ZA-SLMS** | 2.52 | 3.61 | 2.45 | 3.69 | 4.08 | 3.27 |
| **⩽WSPNMF+ZA-SLMS** | 2.21 | 3.70 | 2.24 | 3.47 | 4.38 | 3.20 |

* Supplemented $d_0 = 30$ cm.

(b) Typing with a laptop

| | Subj 1 | Subj 2 | Subj 3 | Subj 4 | Subj 5 | Avg |
|---|---|---|---|---|---|---|
| **Spectrogram [16]** | 12.80 | 10.06 | 8.60 | 12.14 | 13.33 | 11.39 |
| **SSA+ZA-SLMS [40]** | 3.11 | 3.26 | 2.68 | 6.20 | 5.07 | 4.06 |
| **NMF+ZA-SLMS** | 2.93 | 3.73 | 2.82 | 5.47 | 3.50 | 3.69 |
| **SPNMF+ZA-SLMS** | 2.90 | 3.68 | 3.26 | 5.01 | 3.00 | 3.57 |
| **WSPNMF+ZA-SLMS** | 2.46 | 3.11 | 2.43 | 5.05 | 3.68 | 3.35 |

### 4.5.1 Performance Evaluation on HR

Against the activities of sitting still and typewriting with moderate movements, the results of AAE and AAEP on HR estimations of five subjects are summarized in Table 4.1 and Table 4.2, respectively. In Table 4.1(a), when a subject motionlessly sits as possible, the SSA+ZA-SLMS method [40] obtains a moderate average AAE of 3.57 BPM, and our proposal exhibits higher accuracies by reliable heartbeat extraction, of which SPNMF+ZA-SLMS method and WSPNMF+ZA-SLMS method obtain almost same smallest AAEs, 3.18 BPM and 3.19 BPM. To the typewriting accompanying body motion, the performances of the spectrogram method [16] and SSA+ZA-SLMS evidently degrade, in contrast, the proposed three methods (NMF+ZA-SLMS, SPNMF+ZA-SLMS, and WSPNMF+ZA-SLMS) still robustly estimate HR, specifically, the smallest AAE of 3.35 BPM is obtained by WSPNMF+ZA-SLMS. In the existence of MA, WSPNMF can better make use of the difference of sparsity that

Table 4.2: Average absolute error percentage (AAEP) of HR estimation

(a) Sitting still

| | Subj 1 | Subj 2 | Subj 3 | Subj 4 | Subj 5 | Avg |
|---|---|---|---|---|---|---|
| **Spectrogram [16]** | 5.79% | 12.08% | 14.50% | 9.93% | 14.53% | 11.37% |
| **SSA+ZA-SLMS [40]** | 4.29% | 4.61% | 4.35% | 4.21 | 5.62% | 4.62% |
| **NMF+ZA-SLMS** | 3.05% | 4.78% | 3.99% | 4.75% | 5.44% | 4.40% |
| **SPNMF+ZA-SLMS** | 3.35% | 4.48% | 4.13% | 4.71% | 4.27% | 4.19% |
| **WSPNMF+ZA-SLMS** | 3.50% | 4.32% | 4.37% | 3.91% | 4.73% | 4.17% |
| **≤NMF+ZA-SLMS** | 2.54% | 4.79% | 2.35% | 5.31% | 5.40% | 4.08% |
| **≤SPNMF+ZA-SLMS** | 2.66% | 4.68% | 2.30% | 5.24% | 5.08% | 3.99% |
| **≤WSPNMF+ZA-SLMS** | 2.33% | 4.78% | 2.11% | 4.92% | 5.51% | 3.93% |

* Supplemented $d_0 = 30$ cm.

(b) Typing with a laptop

| | Subj 1 | Subj 2 | Subj 3 | Subj 4 | Subj 5 | Avg |
|---|---|---|---|---|---|---|
| **Spectrogram [16]** | 16.54% | 14.11% | 11.47% | 15.52% | 15.43% | 14.61% |
| **SSA+ZA-SLMS [40]** | 3.97% | 4.61% | 3.55% | 8.08% | 5.82% | 5.21% |
| **NMF+ZA-SLMS** | 3.78% | 5.28% | 3.71% | 6.74% | 4.02% | 4.71% |
| **SPNMF+ZA-SLMS** | 3.72% | 5.19% | 4.29% | 6.14% | 3.44% | 4.56% |
| **WSPNMF+ZA-SLMS** | 3.16% | 4.42% | 3.19% | 6.12% | 4.21% | 4.22% |

is more distinct between heartbeat and other sources including motions, further improved measurement accuracy than SPNMF. Table 4.2 lists the AAEP statistics that are basically consistent with the results of Table 4.1. Our proposal acquires better estimations over the spectrogram method and SSA+ZA-SLMS, both under sitting still and typewriting, also, WSPNMF+ZA-SLMS outperforms other methods, respectively obtaining smallest 4.17% and 4.22%.

The estimated HR variabilities by different detection methods are also intuitively illustrated in Fig. 4-8. The interference of respiration and MA severely corrupts the spectrogram method, while, degrades the estimated results of SSA+ZA-SLMS that are highlighted by circles. In contrast, through stably extracting heartbeat component, the HR estimations of proposed three methods overall more approach to ground-truth. In particular, WSPNMF+ZA-SLMS markedly improves the corruptions of SSA+ZA-SLMS, and most faithfully reflects realistic HR variability among all the referred methods.

Table 4.3: Root-mean-square error (RMSE) of RRI estimation [ms]

(a) Sitting still

| | Subj 1 | Subj 2 | Subj 3 | Subj 4 | Subj 5 | Avg |
|---|---|---|---|---|---|---|
| **Spectrogram [16]** | 60 | 163 | 173 | 119 | 167 | 136 |
| **SSA+ZA-SLMS [40]** | 42 | 49 | 43 | 54 | 49 | 47 |
| **NMF+ZA-SLMS** | 29 | 49 | 42 | 52 | 48 | 44 |
| **SPNMF+ZA-SLMS** | 33 | 47 | 42 | 52 | 41 | 43 |
| **WSPNMF+ZA-SLMS** | 33 | 46 | 42 | 43 | 39 | 41 |
| **≤NMF+ZA-SLMS** | 23 | 46 | 16 | 62 | 56 | 41 |
| **≤SPNMF+ZA-SLMS** | 20 | 44 | 17 | 48 | 55 | 37 |
| **≤WSPNMF+ZA-SLMS** | 18 | 44 | 16 | 50 | 53 | 36 |

* Supplemented $d_0 = 30$ cm.

(b) Typing with a laptop

| | Subj 1 | Subj 2 | Subj 3 | Subj 4 | Subj 5 | Avg |
|---|---|---|---|---|---|---|
| **Spectrogram [16]** | 218 | 188 | 142 | 203 | 183 | 187 |
| **SSA+ZA-SLMS [40]** | 42 | 44 | 36 | 68 | 47 | 47 |
| **NMF+ZA-SLMS** | 37 | 49 | 39 | 67 | 35 | 45 |
| **SPNMF+ZA-SLMS** | 42 | 50 | 43 | 61 | 31 | 45 |
| **WSPNMF+ZA-SLMS** | 34 | 46 | 32 | 66 | 37 | 43 |

### 4.5.2 Performance Evaluation on RRI

To further perform accuracy assessment, the RMSEs of our proposal are calculated, by transforming estimated HR to RRI based on Eq. (4.4). The summarized results of RMSE in Table 4.3 also demonstrate the performance superiority of the proposed three methods (NMF+ZA-SLMS, SPNMF+ZA-SLMS, and WSPNMF+ZA-SLMS) that separate sources, against various activities of sitting still and typewriting. Particularly for WSPNMF+ZA-SLMS that penalizes weighted sparseness constraints, it respectively reaches the most desired RMSEs, only 41 ms and 43 ms.

Supplementarily, to eliminate the difference of ranging to typing condition, the estimated results by our proposal when subjects sit still at 30 cm-range, are also respectively listed in Tables 4.1–4.3. One can find that the estimations on sitting still evidently outperform those on typing in most cases including averages, which revalidates the influence of MA to HR measurement.

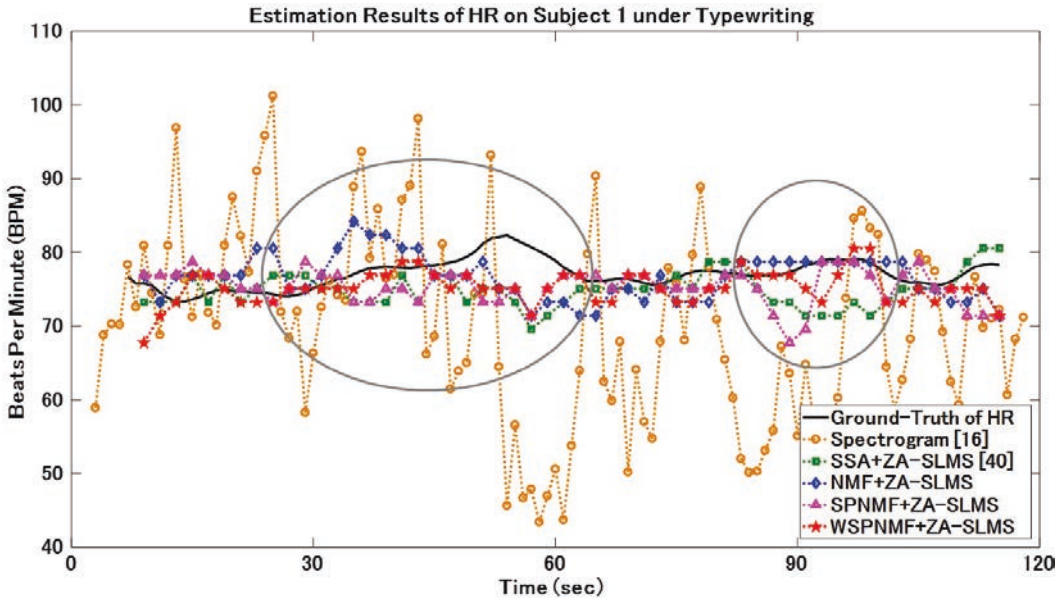


Figure 4-8: Intuitive comparison of HR estimation results of Subject 1 under typewriting, by various heartbeat detection methods

**Method 5** Projection function invoked by SPNMF or WSPNMF: $P(\mathbf{y}, L_1, L_2)$

**Input:** $\mathbf{y}$, $L_1$, $L_2$

**Output:** The closest non-negative vector to $\mathbf{y}$ with joint constraint of $\ell_1$-norm and $\ell_2$-norm, denoted as $\hat{\mathbf{s}}(n)$

Set zeros-set $Z = \varnothing$ and $n = 1$. Initiatively project $\mathbf{y}$ onto $\ell_1$-norm hypersphere as follows,

$$s_i(n) = y_i + \Big) L_1 \quad \Big[ \quad y_i \Big( /N, \; i \; / \; \} 1, \times\times\times, N| \; ,$$

where $N$ is the dimensionality of $\mathbf{y}$.

**loop**

Step i. Project $\mathbf{s}(n)$ to the closest intersection of $\ell_1$-norm and $\ell_2$-norm.

$$m_i = \begin{cases} L_1 / \left(N \quad \text{card}(Z)\right), \text{ if } i \; / \; Z \\ 0, \text{ if } i \; / \; Z \end{cases} ,$$

where $L_1$-induced $\mathbf{m}$ is termed midpoint, and $\text{card}(Z)$ represents the number of elements in $Z$. To satisfy the $\ell_2$-norm constraint, a quadratic equation $a\mathbf{x}^2 + b\mathbf{x} + c = 0$ ($a$, $b$, and $c$ are constants) is required to solve,

$$a = \Big[ \quad d_i^2; \; b = \mathbf{d}^{\mathrm{T}} \mathbf{s}(n); \; c = \Big[ \quad s_i^2(n) \quad L_2,$$

where $\mathbf{d} = \mathbf{s}(n) \quad \mathbf{m}$.

$$\alpha = \Big) \quad b + \nabla \overline{b^2 \quad 4ac} \Big( /(2a),$$

$$\mathbf{s}(n+1) = \mathbf{s}(n) + \alpha \left(\mathbf{s}(n) \quad \mathbf{m}\right).$$

*Case a:* If all the coefficients of $\mathbf{s}(n+1)$ are non-negative, return the current $\mathbf{s}(n+1)$ as output $\hat{\mathbf{s}}(n)$.

**if** $s_i(n+1) \geqslant 0, \cup i$ **then**

**break**

*Case b:* If NOT all the coefficients of $\mathbf{s}(n+1)$ are non-negative, Step ii. and Step iii. proceed.

**else**

Step ii. Fix the subtractive coefficients of $\mathbf{s}(n+1)$ at zero.

$$Z = Z \; \{ \; \} i \| s_i(n+1) < 0| \; ,$$

$$s_i(n+1) = 0, \cup i \; / \; Z.$$

Step iii. Prune non-negative $\mathbf{s}(n+1)$ by $L_1$.

$$r = \Big) \Big[ \quad s_i(n+1) \quad L_1 \Big( / \left(N \quad \text{card}(Z)\right),$$

$$s_i(n+1) = s_i(n+1) \quad r, \cup i \; / \; Z.$$

**end if**

$$n = n + 1.$$

**end loop**

**Method 6** WSPNMF algorithm for BSS

**Input:** **X**

**Output:** **W**, **H**

1: Initialize non-negative **W** and **H** by random Gaussian distribution, choose number of sources $I$ as three and upper bound of iterations $C_{\mathrm{WSPNMF}}$. Set $S_{\mathbf{H}}$ / $[0,1]$, $\Lambda = \mathbf{1}$, $\delta$, $\eta$, and $n = k = f = t = 1$.

$$L_1 = \overline{T} \quad \nabla \overline{T} \quad 1 S_{\mathbf{H}},$$

where $T$ is the number of columns of **H**. Initially invoke the projection function,

$$\mathbf{h}_k(n) = P\left(\mathbf{h}_k(n), L_1, 1\right), \; k \; / \; 1, \times\times\times, I| \; .$$

2: **while** $n \leqslant C_{\mathrm{WSPNMF}}$ **do**

$$W_{fk}(n+1) = W_{fk}(n) \frac{XH^{\mathrm{T}}_{fk}}{[WHH^{\mathrm{T}}]_{fk}}.$$

3: Implement additive gradient descent to **H** as follows,

$$H_{kt}(n+1) = H_{kt}(n) \quad \mu W^{\mathrm{T}}(WH \quad X)_{kt},$$

4: Introduce $\lambda_k$ to weight the value of $L_1$ when the projection function is invoked.

$$\mathbf{h}_k(n+1) = P\left(\mathbf{h}_k(n+1), \lambda_k L_1, 1\right).$$

5: **if** $n = C_{\mathrm{WSPNMF}}/2$ **then**

$$R_k = 1/\mathrm{std}\left(\mathrm{diff}\left(\mathbf{h}_k(n+1)\right)\right),$$

$$\lambda_k = \delta + \eta R_k.$$

6: **end if**

$$n = n + 1.$$

7: **end while**

# Chapter 5

# Conclusions and Future Work

## 5.1 Conclusions

This thesis has first proposed a novel method for heart rate (HR) estimation via Doppler radar, through reconstructing robustly a heartbeat spectrum with high-resolution, by a stochastic gradient descent (SGD) manner, combating the noises from respiration and body motion. Based on the SGD, first, the zero-attracting sign least-mean-square (ZA-SLMS) algorithm is applied to realize sparse spectrum reconstruction (SSR) by restricting gradient updating. Then, an improved ZA-SLMS (IZA-SLMS) algorithm is further proposed, to better cope with different subjects' activities. Finally, the incorporation of time-window-variation (TWV) in IZA-SLMS enhances the stability of heartbeat detection, with moderately increased computational load. Relying on the high-resolution spectrum reconstruction and robust noise suppression in frequency domain, the proposed SSR obtained improved accuracy of HR estimation. Specifically, the stable HR measurement by the IZA-SLMS with TWV reaches the smallest average error. Taking account of the residual noise in Doppler signal after the relatively rough temporal signal decomposition for heartbeat extraction, which may directly corrupt the effect of SSR, a new signal processing approach in time domain is needed.

Moreover, an unsupervised blind source separation (BSS) approach is further proposed, to stably extract heartbeat component even moderate body motion occurs,

based on a simple non-negative matrix factorization (NMF) structure. The proposed BSS is of great value due to three main superiorities: It (i) omits the training phase that most learning methods require; (ii) adopts simple-structured NMF algorithms that only focus on local representations of data; (iii) enables source separation by single-channel input. Experiments verified the performance improvements of heart rate (HR) estimation by our proposal, combining with the SSR and the BSS, over the other typical existing detection methods. In particular, the sparseness constraints introduced in sparse NMF (SPNMF) and weighted sparse NMF (WSPNMF) algorithms furthest reduced errors, by exploiting the temporal sparsity of heartbeat.

## 5.2 Future Work

In view of the remarkable robustness and practicability of our proposed method with the approaches of SSR and BSS, as the next work, we will attempt it in specific applications that need easy-to-use and long-term HR detection accompanying body motion, such as:

- Sleeping monitoring and scoring in clinical environments
- HR tracking to a driver
- Smart homes that monitor vital signs including respiration

We believe the advantages of our proposal can benefit the achievement of the mentioned appealing applications, and the possible improvement of algorithms is also taken into account. In particular, through training subjects' daily data, the prevailing machine learning technique probably further enhances the heartbeat extraction in BSS, even in more rigorous conditions, e.g., HR monitoring during intensive physical exercise.

# Bibliography


[1] T. Ohtsuki, "(invited paper) A smart city based on ambient intelligence," *IEICE Trans. Commun.*, vol. E100.B, no. 9, pp. 1547–1553, Sep. 2017.

[2] C. Li, V. M. Lubecke, O. B.-Lubecke, and J. Lin, "(invited paper) A review on recent advances in Doppler radar sensors for noncontact healthcare monitoring," *IEEE Trans. Microw. Theory Techn.*, vol. 61, no. 5, pp. 2046–2060, Apr. 2013.

[3] Y. Lee, J.-Y. Park, Y.-W. Choi, H.-K. Park, S.-H. Cho, S. H. Cho, and Y.-H. Lim, "A novel non-contact heart rate monitor using impulse-radio ultra-wideband (IR-UWB) radar technology," *Scientific Reports*, vol. 8, no. 13053, Aug. 2018.

[4] M. Sekine and K. Maeno, "Non-contact heart rate detection using periodic variation in Doppler frequency," in *IEEE Sensors Appl. Symp.*, Feb. 2011, pp. 318–322.

[5] C. Song, K. Liu, X. Zhang, L. Chen, and X. Xian, "An obstructive sleep apnea detection approach using a discriminative hidden Markov model from ECG signals," *IEEE Trans. Biomed. Eng.*, vol. 63, no. 7, pp. 1532–1542, July 2016.

[6] A. Temko, "Accurate heart rate monitoring during physical exercises using PPG," *IEEE Trans. Biomed. Eng.*, vol. 64, no. 9, pp. 2016–2024, Sep. 2016.

[7] J. Park, J. Ham, S. Park, D.-H. Kim, S.-J. Park, H. Kang, and S.-O. Park, "Polyphase-basis discrete cosine transform for real-time measurement of heart rate with CW Doppler radar," *IEEE Trans. Microw. Theory Techn.*, vol. 66, no. 3, pp. 1644–1659, Mar. 2018.

[8] L. Fanucci, "Sensing devices and sensor signal processing for remote monitoring of vital signs in CHF patients," *IEEE Trans. Instrum. Meas.*, vol. 62, no. 3, pp. 553–569, Mar. 2013.

[9] W. Hu, Z. Zhao, Y. Wang, H. Zhang, and F. Lin, "Noncontact accurate measurement of cardiopulmonary activity using a compact quadrature Doppler radar sensor," *IEEE Trans. Biomed. Eng.*, vol. 61, no. 3, pp. 725–735, Mar. 2014.

[10] K. J. Lee, C. Park, and B. Lee, "Tracking driver's heart rate by continuous-wave Doppler radar," in *38th Annu. IEEE Int. Eng. Med. Biol. Soc. Conf.*, Aug. 2016, pp. 5417–5420.

[11] E. M. Staderini, "UWB radars in medicine," *IEEE Aerosp. Electron. Syst. Mag.*, vol. 17, no. 1, pp. 13–18, Jan. 2002.

[12] K.-M. Chen, Y. Huang, J. Zhang, and A. Norman, "Microwave life-detection systems for searching human subjects under earthquake rubble or behind barrier," *IEEE Trans. Biomed. Eng.*, vol. 47, no.1, pp. 105–114, Jan. 2000.

[13] M. Nosrati and N. Tavassolian, "High-accuracy heart rate variability monitoring using Doppler radar based on Gaussian pulse train modeling and FTPR algorithm," *IEEE Trans. Microw. Theory Techn.*, vol. 66, no. 1, pp. 556–567, Jan. 2018.

[14] J. Tu and J. Lin, "Fast acquisition of heart rate in noncontact vital sign radar measurement using time-window-variation technique," *IEEE Trans. Instrum. Meas.*, vol. 65, no. 1, pp. 112–122, Jan. 2016.

[15] E. Mogi and T. Ohtsuki, "Heartbeat detection with Doppler sensor using adaptive scale factor selection on learning," in *IEEE 26th Annual Int. Symp. Personal, Indoor, Mobile Radio Commun.*, Aug. 2015, pp. 2166–2170.

[16] E. Mogi and T. Ohtsuki, "Heartbeat detection with Doppler radar based on spectrogram," in *IEEE Int. Conf. Commun.*, May 2017, pp. 1–6.

[17] B.-K. Park, O. B.-Lubecke, and V. M. Lubecke, "Arctangent demodulation with dc offset compensation in quadrature Doppler radar receiver systems," *IEEE Trans. Microw. Theory Techn.*, vol. 55, no. 5, pp. 1073–1079, May 2007.

[18] Z. Wu and N. E. Huang, "Ensemble empirical mode decomposition: a noise-assisted data analysis method," *Adv. in Adapt. Data Anal.*, vol. 1, no. 1, pp. 1–41, Jan. 2009.

[19] C. Li and J. Lin, "Complex signal demodulation and random body movement cancellation techniques for non-contact vital sign detection," in *IEEE MTT-S Int. Microw. Symp. Digit.*, Jun. 2008, pp. 567–570.

[20] C. Gu, C. Li, J. Lin, J. Long, J. Huangfu, and L. Ran, "Instrument-based noncontact Doppler radar vital sign detection system using heterodyne digital quadrature demodulation architecture," *IEEE Trans. Instrum. Meas.*, vol. 59, no. 6, pp. 1580–1588, June 2010.

[21] P. Li and D. Wang, "A quadrature Doppler radar system for sensing human respiration and heart rates," in *10th Proc. Int. Conf. Signal Process.*, Oct. 2010, pp. 2235–2238.

[22] J. Tu and J. Lin, "Respiration harmonics cancellation for accurate heart rate measurement in non-contact vital sign detection," in *IEEE MTT-S Int. Microw. Symp. Digit.*, Jun. 2013, pp. 1–3.

[23] A. Tariq and H. G. Shiraz, "Vital signs detection using Doppler radar and continuous wavelet transform," in *Proc. 5th European Conf. Antennas Propagation*, Apr. 2015, pp. 285–288.

[24] M. He, Y. Nian, and B. Liu, "Noncontact heart beat signal extraction based on wavelet transform," in *Proc. 8th Biomed. Eng. Informat.*, Oct. 2015, pp. 209–213.

[25] S. Tomii and T. Ohtsuki, "Heartbeat detection by using Doppler radar with wavelet transform based on scale factor learning," in *IEEE Int. Conf. Commun.*, June 2015, pp. 483–488.

[26] M. Li and J. Lin, "Wavelet-transform-based data-length-variation technique for fast heartrate detection using 5.8-GHz CW Doppler radar," *IEEE Trans. Microw. Theory Techn.*, vol. PP, no. 99, pp. 1–9, July 2016.

[27] G. Lu, F. Yang, X. Jing, and J. Wang, "Contact-free measurement of heartbeat signal via a doppler radar using adaptive filtering," in *Int. Conf. Image Anal. and Signal Process.*, Apr. 2010, pp. 89–92.

[28] C. Li and J. Lin, "Recent advances in Doppler radar sensors for pervasive healthcare monitoring," in *Proc. 22nd Asia-Pacific Microw. Conf.*, Dec. 2010, pp. 283–290.

[29] W. Massagram, V. M. Lubecke, A. H.-Madsen, and O. B.-Lubecke, "Assessment of heart rate variability and respiratory sinus arrhythmia via Doppler radar," *IEEE Trans. Microw. Theory Tech.*, vol. 57, no. 10, pp. 2542–2549, Oct. 2009.

[30] Z. Zhang, Z. Pi, and B. Liu, "TROIKA: A general framework for heart rate monitoring using wrist-type photoplethysmographic signals during intensive physical exercise," *IEEE Trans. Biomed. Eng.*, vol. 62, no. 2, pp. 522–531, Feb. 2015.

[31] J. M. M. Torres, A. Ghosh, E. A. Stepanov, and G. Riccardi, "Heal-T: An efficient PPG-based heart-rate and IBI estimation methodduring physical exercise," in *24th European Signal Proc. Conf.*, Aug. 2016, pp. 1438–1442.

[32] M. F. Duarte and R. G. Baraniuk, "Spectral compressive sensing," *Applied Computational Harmonic Anal.*, vol. 35, no. 1, pp. 111–129, 2013.

[33] G. Gui, L. Xu, W. Ma, and B. Chen, "Robust adaptive sparse channel estimation in the presence of impulsive noises," in *IEEE Int. Conf. Digit. Signal Process.*, July 2015, pp. 628–632.

[34] J. Jin, Y. Gu, and S. Mei, "A stochastic gradient approach on compressive sensing signal reconstruction based on adaptive filtering framework," *IEEE J. Sel. Top. Signal Process.*, vol. 4, no. 2, pp. 409–420, Apr. 2010.

[35] E. J. Candes, J. Romberg, and T. Tao, "Robust uncertainty principles: exact signal reconstruction from highly incomplete frequency information," *IEEE Trans. Inf. Theory*, vol. 52, no. 2, pp. 489–509, Feb. 2006.

[36] D. L. Donoho, "Compressed sensing," *IEEE Trans. Inf. Theory*, vol. 52, no. 4 pp. 1289–1306, Apr. 2006.

[37] I. F. Gorodnitsky and B. D. Rao, "Sparse signal reconstruction from limited data using FOCUSS: a re-weighted minimum norm algorithm," *IEEE Trans. Signal Process.*, vol. 45, no. 3, pp. 600–616, Mar. 1997.

[38] S. F. Cotter, B. D. Rao, K. Engan, and K. K.-Delgado, "Sparse solutions to linear inverse problems with multiple measurement vectors," *IEEE Trans. Signal Process.*, vol. 53, no. 7, pp. 2477–2488, July 2005.

[39] C. Ye, G. Gui, S. Matsushita, and L. Xu, "Robust stochastic gradient-based adaptive filtering algorithms to realize compressive sensing against impulsive interferences," in *28th Chinese Control Decision Conf.*, May 2016, pp. 1946–1951.

[40] C. Ye, K. Toyoda, and T. Ohtsuki, "Robust heartbeat detection with Doppler radar based on stochastic gradient approach," in *IEEE Int. Conf. Commun.*, May 2018, pp. 1–6.

[41] Y. Ye, Y. Cheng, W. He, M. Hou, and Z. Zhang, "Combining nonlinear adaptive filtering and signal decomposition for motion artifact removal in wearable photoplethysmography," *IEEE Sensors J.*, vol. 16, no. 19, pp. 7133–7141, Oct. 2016.

[42] N. Golyandina and A. Zhigljavsky, *Singular spectrum analysis for time series*. Berlin, Germany: Springer-Verlag, 2013.

[43] P. Stoica and R. L. Moses, *Spectral analysis of signals*. Pearson/Prentice Hall Upper Saddle River, NJ, 2005.

[44] G. Gui. L. Xu, and N. Shimoi, "Stable sparse channel estimation algorithm under non-Gaussian noise environments," in *21st Asia-Pacific Conf. Commun.*, Apr. 2015, pp. 561–565.

[45] D. D. Lee and H. S. Seung, "Learning the parts of objects by non-negative matrix factorization," *Nature*, vol. 401, pp. 788–791, Oct. 1999.

[46] D. D. Lee and H. S. Seung, "Algorithms for non-negative matrix factorization," in *13th Int. Conf. Neural Inform. Process. Syst.*, 2000, pp. 535–541.

[47] Z. Huang, A. Zhou, and G. Zhang, *Non-negative matrix factorization: A short survey on methods and applications*. Berlin, Germany: Springer-Heidelberg, 2012.

[48] Y.-X. Wang and Y.-J. Zhang, "Nonnegative matrix factorization: A comprehensive review," *IEEE Trans. Knowledge and Data Eng.*, vol. 25, no. 6, pp. 1336–1353, May 2013.

[49] J. R. Hershey, Z. Chen, J. L. Roux, and S. Watanabe, "Deep clustering: Discriminative embeddings for segmentation and separation," in *IEEE Int. Conf. Acoust., Speech and Signal Process.*, Mar. 2016, pp. 31–35.

[50] P. O. Hoyer, "Non-negative matrix factorization with sparseness constraints," *J. Mach. Learn. Res.*, vol. 5, pp. 1457–1469, Dec. 2004.

[51] G. Shah, P. Koch, and C. B. Papadias, "On the blind recovery of cardiac and respiratory sounds," *IEEE J. Biomed. Health Inform.*, vol. 19, no. 1, pp. 151–157, Jan. 2015.

[52] R. Yan, C. Zhang, K. Spruyt, L. Wei, Z. Wang, L. Tian, X. Li, T. Ristaniemi, J. Zhang, and F. Cong, "Multi-modality of polysomnography signals' fusion for automatic sleep scoring," *Biomed. Signal Process. Control*, vol. 49, pp. 14–23, Mar. 2019.

[53] C. Ye, K. Toyoda, and T. Ohtsuki, "Non-negative matrix factorization-based blind source separation for non-contact heartbeat detection," in *IEEE Int. Conf. Commun.*, May 2019, to appear.

[54] C. Lin and E. Hasting, "Blind source separation of heart and lung sounds based on nonnegative matrix factorization," in *Int. Symp. Intell. Signal Process. Commun. Syst.*, Nov. 2013, pp. 731–736.

[55] C. Mert and A. Milnikov, "Singular spectrum analysis method as a universal filter," in *Proc. 5th Int. Conf. Appl. Inf. Commun. Tech.*, Oct. 2011, pp. 1–5.

[56] C. F. N. Cowan and P. M. Grant, *Adaptive filters*. Englewood Cliffs, NJ: Prentice-Hall, 1985.

[57] P. S. R. Diniz, *Adaptive filtering*. 4th ed. Boston, MA, USA: Kluwer, 2013.

[58] Y. Chen, Y. Gu, and A. O. Hero, "Sparse LMS for system identification," in *IEEE Int. Conf. Acoust., Speech and Signal Process.*, Apr. 2009, pp. 3125–3128.

[59] D. Middleton, "Non-Gaussian noise models in signal processing for telecommunications: new methods an results for class A and class B noise models," *IEEE Trans. Inf. Theory*, vol. 45, no. 4, pp. 1129–1149, May 1999.

[60] K. Pelekanakis and M. Chitre, "Adaptive sparse channel estimation under symmetric alpha-stable noise," *IEEE Trans. Inf. Theory*, vol. 13, no. 6, pp. 3183–3195, June 2014.

[61] M. A. Chitre, J. R. Potter, and S.-H. Ong, "Optimal and near-optimal signal detection in snapping shrimp dominated ambient noise," *IEEE J. Ocean. Eng.*, vol. 31, no. 2, pp. 497–503, Apr. 2006.

[62] S. Zhang and J. Zhang, "Modified variable step-size affine projection sign algorithm," *Electronics Letters*, vol. 49, no. 20, pp. 1264–1265, Sep. 2013.

# Appendix A

# Publication List

## A.1 Journals

[1] C. Ye, G. Gui, S. Matsushita, and L. Xu, "Block sparse signal reconstruction using block-sparse adaptive filtering algorithms," *J. Adv. Comput. Intell. Inform.*, vol.20, no.7, pp.1119–1126, Dec. 2016.

[2] C. Ye, G. Gui, and L. Xu, "Compressive sensing signal reconstruction using L0-norm normalized least mean fourth algorithms," *Circuits Syst. Signal Process.*, vol.37, no.4, pp.1724–1752, Apr. 2018.

[3] C. Ye, G. Gui, L. Xu, and T. Ohtsuki, "Recovery of block-structured sparse signal using block-sparse adaptive algorithms via dynamic grouping," *IEEE Access*, vol.6, no.1, pp. 56069–56083, Dec. 2018.

[4] C. Ye, K. Toyoda, and T. Ohtsuki, "A stochastic gradient approach for robust heartbeat detection with Doppler radar using time-window-variation technique," *IEEE Trans. Biomed. Eng.*, vol.66, no.6, pp. 1730–1741, June 2019.

[5] C. Ye, K. Toyoda, and T. Ohtsuki, "Blind source separation on non-contact heartbeat detection by non-negative matrix factorization algorithms," *IEEE Trans. Biomed. Eng.*, online first, pp. 1–13, May 2019.

## A.2 Conferences Proceedings (peer-reviewed)

[1] C. Ye, G. Gui, L Xu, and N. Shimoi, "Improved adaptive sparse channel estimation using re-weighted L1-norm normalized least mean fourth algorithm," in *54th Annual Conf. of the Society of Instrument Control Eng.*, July 2015, pp. 689–694.

[2] C. Ye, G. Gui, S. Matsushita, and Li Xu, "Robust stochastic gradient-based adaptive filtering algorithms to realize compressive sensing against impulsive interferences," in *28th Chinese Control Decision Conf.*, May 2016, pp. 1946–1951.

[3] C. Ye, G. Gui, S. Matsushita, and Li Xu, "Block sparse signal reconstruction using block-sparse adaptive filtering algorithms," in *11th Japan-China Int. Workshop on Infor. Tech. Control Applications*, Aug. 2016.

[4] C. Ye, K. Toyoda, and T. Ohtsuki, "Robust heartbeat detection with Doppler radar based on stochastic gradient approach," in *IEEE Int. Conf. Commun.*, May 2018, pp. 1–6.

[5] C. Ye, K. Toyoda, and T. Ohtsuki, "Improved sparse adaptive algorithms for accurate non-contact heartbeat detection using time-window-variation technique," in *40th Int. Conf. the IEEE Eng. in Medicine Biology Society*, July 2018, pp. 1–6.

[6] C. Ye, K. Toyoda, and T. Ohtsuki, "Non-negative matrix factorization-based blind source separation for non-contact heartbeat detection," in *IEEE Int. Conf. Commun.*, May 2019, to appear.

## A.3 Conferences Proceedings (Japanese, without peer-review)

[1] 葉臣, 桂冠, 松下慎也, 徐粒, Improved adaptive sparse channel estimation using re-weighted L1-norm normalized least mean fourth algorithm, 平成 27 年度電気関係学会東北支部連合大会, 岩手県立大学滝沢キャンパス, 滝沢, 2015 年 8 月 27 日発表済.

[2] 葉臣, 桂冠, 松下慎也, 徐粒, Improved cluster-structured sparse signal recovery using iterative-grouping-based block-sparse adaptive filtering algorithms, 計測自動制御学会東北支部第 303 回研究集会, 秋田県立大学本荘キャンパス, 由利本荘, 2016 年 7 月 15 日発表済.

[3] 小崎大介, 葉臣, 松下慎也, 徐粒, 適応アルゴリズムを用いた圧縮センシングと磁気共鳴画像応用への検討, 平成 28 年度電気関係学会東北支部連合大会, 東北工業大学八木山キャンパス, 仙台, 2016 年 8 月 31 日発表済.

[4] 葉臣, 桂冠, 松下慎也, 徐粒, Robust recovery of inexact block-sparse signals by block version of sparse adaptive filtering algorithms, 平成 28 年度電気関係学会東北支部連合大会, 東北工業大学八木山キャンパス, 仙台, 2016 年 8 月 31 日発表済.

[5] 葉臣, 豊田健太郎, 大槻知明, 確率的勾配降下法を用いたドップラーレーダによるロバストな心拍検出, 電子情報通信学会ソサイエティ大会, 東京都市大学, 東京, 2017 年 9 月 14 日発表済.

[6] 葉臣, 豊田健太郎, 大槻知明, ロバストスパース適応アルゴリズムに基づくドップラーレーダによる非接触心拍検出, 電子情報通信学会ヘルスケア・医療情報通信技術研究会 (MICT), 機械振興会館, 東京, 2018 年 3 月 16 日発表済.

[7] 葉臣, 豊田健太郎, 大槻知明, [依頼講演] スパース適応アルゴリズムに基づく非接触心拍検出, 電子情報通信学会無線システム研究会 (RCS), 岩手大学, 盛岡, 2018 年 8 月 9 日発表済.

## A.4 Patents

[1] T. Ohtsuki and C. Ye, "Heartbeat detection system and method," Keio University, Application Number: 0000002992, Publication Number: 2018-14373, Jan. 2018.

## A.5 Awards

[1] Nov. 2015 Student Awards: Encouragement Prize (IEEE Sendai Section)

[2] 2019 年 3 月 第 34 回 電気通信普及財団 テレコムシステム技術学生賞佳作